ACS NANO

www.acsnano.org

ARTICLE

Exosome Heterogeneity Affects the Distal "Barrier-Crossing" Trafficking of Exosome Encapsulated Quantum Dots

Di Wu, Hang Sun, Bingwei Yang, Erqun Song, Yang Song,* and Weihong Tan

Cite This: https://doi.org/10.1021/acsnano.3c09378

Read Online

ACCESS | Metrics & More | Article Recommendations | Supporting Information

ABSTRACT: The biological activities of nanoparticles (NPs), which include endocytosis by macrophages and subsequent intracellular degradation and/or release, transfer to other cells, or translocation across tissue barriers, highly depend on their fate in living organisms. Yet, translocation across barriers, especially the distal "barrier-crossing" trafficking of NPs, is still unclear. The exosome (Exo) plays a crucial role in intercellular communication and biological barrier trafficking. Here, we report that ZnCdSe@ZnS quantum dots (QDs), as a representation of NPs in biomedical applications, could cross the blood-brain barrier and approach the mouse brain via active Exo encapsulation. By employing multiple techniques, we demonstrated that QDs were internalized by macrophages (J774A.1) and tumor cells (HeLa) and then released to the extracellular environment along with Exo. Exo encapsulation facilitates the distal barrier-crossing trafficking of QDs *in vivo*, while Exo biogenesis inhibitor GW4869 suppressed the QDs enriched in the brains of mice with a 4T1-Luc breast cancer xenograft. Interestingly, Exo heterogeneity affects the distal trafficking of enveloped QDs. Exo derived from tumorous HeLa cells, not macrophages, that were enriched in functional proteins with cell adhesion, cell migration, axon guidance, and cell motility, showed a better capacity for the remote trafficking of QDs. This study proposes Exo as a vehicle to deliver exogenous NPs to translocate across the distal barrier and provides further information for biomedical application and the risk assessment of NPs.

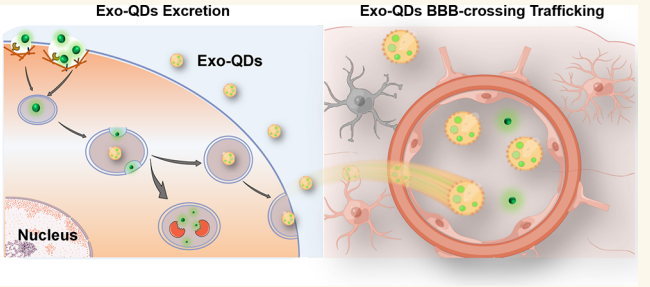

KEYWORDS: *exosome, quantum dots, intercellular trafficking, blood-brain barrier, heterogeneity*

INTRODUCTION

The rapid development of nanotechnology is responsible for the deliberate and accidental release of anthropogenic nanoparticles (NPs) into the environment.[1] With the ubiquitous existence of natural and anthropogenic NPs in the atmosphere, hydrosphere, and biosphere,[2] human exposure to NPs is inevitable and has adverse consequences, becoming a significant global public issue.[3] Our recent studies suggested that once introduced into the mice through different pathways, NPs, such as silica NPs (15 nm),[4] anionic nanoplastic NPs (25 nm),[5] and two-dimensional MoS_2 nanosheets (500 nm),[6] could interact with complicated biological barriers *in vivo* and accumulated in vital organs to cause tissue damage. And no consensus has established the strategies used by NPs to cross these complicated biological barriers. Notably, anionic nanoplastic NPs crossing the blood-brain barrier (BBB) by inducing endothelial leakiness and damage the integrity of the barrier,[5] and commercial silica nanoparticles could also cause severe endothelial leakiness.[7] Multiple studies have clearly shown that NPs could enter the brain, and two groups of researchers have expounded on this subject. Toxicologists, for example, chose to investigate how environmental NPs (e.g., airborne particulate matter) become the drivers of neurological disorders/diseases,[8,9] while pharmacologists, on the other hand, seek optimum tactics to deliver nanosized therapeutics and/or diagnostic probes to the brain.[10] Although both have achieved some progress, the detailed mechanism(s) explaining how NPs actively break through the BBB need(s) to be further understood.

The exosome (Exo) is a cup-shaped membrane-derived vesicle with a typical lipid bilayer that ranges from 30 to 150 nm.[11] Long viewed as specifically secreted vesicles for

Received: September 27, 2023
Revised: February 5, 2024
Accepted: February 8, 2024

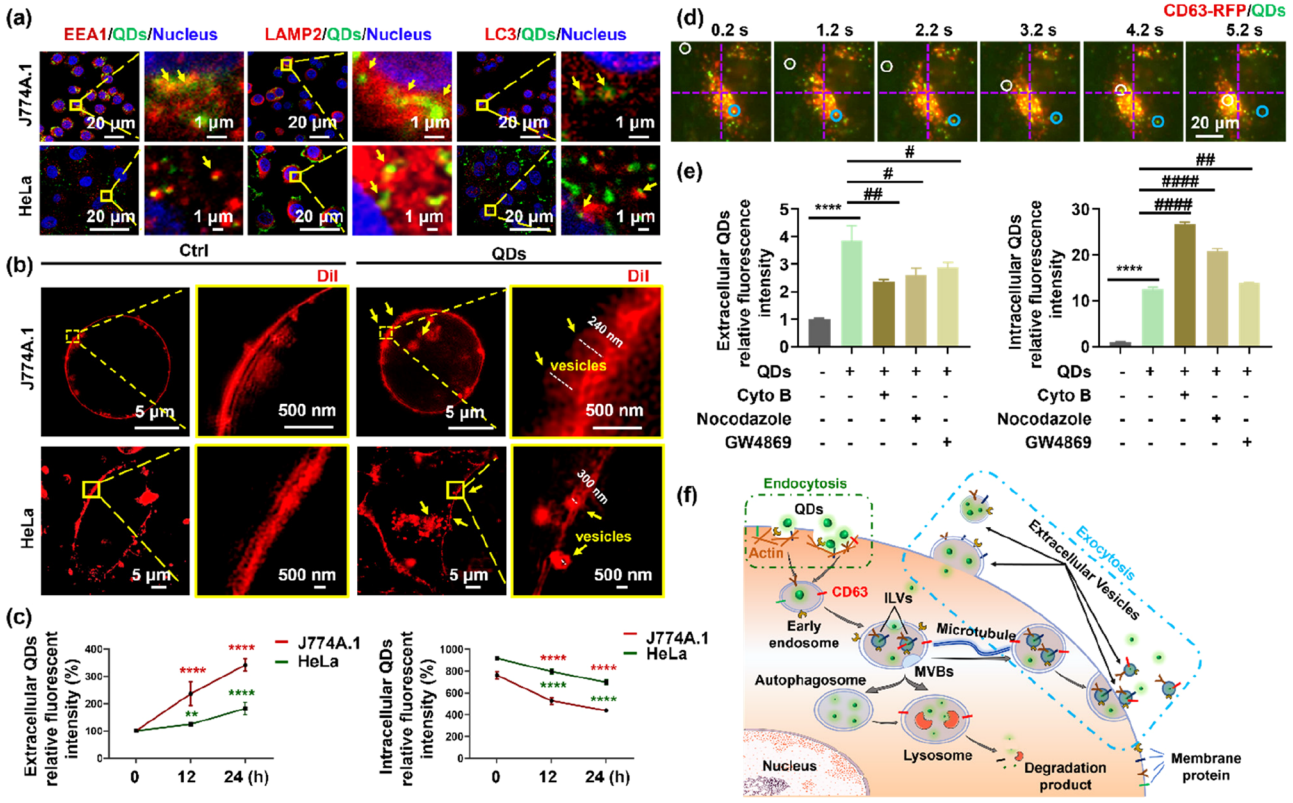

Figure 1. Excretion of QDs via EV encapsulation. (a) Immunofluorescence of EEA1 (left), LAMP2 (middle), and LC3 (right) in J774A.1 and HeLa cells. Cells were incubated with 10 nM QDs (green) for 2 h, and then cells were fixed, permeabilized, blocked, and probed with primary antibodies overnight at 4 °C. Next, cells were incubated with a secondary antibody conjugated with Cy3 (red) for 2 h. Nuclei (blue) were stained with Hoechst 33342. Intracellular QDs were imaged by CLSM. Yellow arrowheads indicate the colocalization of QDs and vesicles. Scale bars, 20 μm and 1 μm. (b) Extracellular vesicle image of J774A.1 and HeLa cells. After incubation with QDs for 12 h, J774A.1 and HeLa cells were fixed, and DiI (red) was used to stain the cell membrane. N-SIM images of vesicles were captured. Scale bars, 5 μm and 500 nm. (c) The release of intracellular QDs. Following incubation with 10 nM QDs for 12 h, a QDs-free culture medium was used to replace the medium (0 h). After indicated incubation times (12, 24 h), cells and cell supernatants were respectively collected. The extracellular QDs' fluorescence intensity in the supernatant was analyzed by a microplate reader, and the intracellular QDs were detected by flow cytometry. All data are means ± SD (n = 3). ANOVA analysis. $^{**}p < 0.01$, $^{****}p < 0.0001$(vs. untreated cells). (d) Time-lapse images were imaged with CLSM in no-delay mode after treatment of 10 nM QDs in CD63-RFP-HeLa cells for 2 h. Fiji plugin tracking was used to analyze the trafficking of QDs. White circle represents the inward movement of QDs, and blue circle represents the outward movement of QDs. Scale bar, 20 μm. (e) Inhibitors affected the secretion of intracellular QDs. Supernatants and cells were collected respectively to detect fluorescence intensity. All data are means ± SD (n = 3). An unpaired t-test was used. $^{****}p < 0.0001$, $^{\#}p < 0.05$, $^{\#\#}p < 0.01$, $^{\#\#\#\#}p < 0.0001$. (f) Schematic illustration of QDs encapsulated in endocytic vesicles for degradation or exocytosis.

intercellular communication, Exo has shown excellent biocompatibility, a long-circulating time, and the intrinsic ability to target deep tissues.[12,13] By delivering bioactive cargoes, e.g., proteins, nucleic acids, lipids, and metabolites derived from parental cells,[14−16] Exo could transfer messages between cells in the local microenvironment and those in distant sites as the primary carrier of multiple signal molecules to influence tissue physiological function, ultimately involved in various biological processes.[15] Practically, tumor-derived Exo are able to modulate autocrine, juxtracrine, and paracrine signaling pathways and play an irreplaceable role in the metastatic cascade of cancer recurrence and metastasis. Thus, tumor-derived Exo has potent applications in the clinic as a therapeutic, diagnostic, and prognostic tool.[17,18]

Exo was used back in 2011 to deliver therapeutics to the brain by intravenous injection.[19] The molecular composition and heterogeneity of Exo will implicate their biological and therapeutic effects.[20] Tumor-derived Exo can impair endothelial cell junctions and thus increase vascular permeability, establishing a favorable microenvironment for premetastatic niche formation and metastasis.[21,22] Apparently, BBB endothelial cells are highly responsive to Exo from some cell sources (stem cells, neural origin, and macrophages), which leads to higher BBB penetration of these Exo.[23] In parallel, researchers also proved that cargoes could be packaged into Exo during their biogenesis.[24−28] However, the loading of NPs cargoes by Exo was mainly performed in cultured cells rather than animals, and whether different cell types derived Exo encapsulation can assist NPs in passing through the BBB needs further verification. Moreover, it is currently unknown whether NPs can be similarly encapsulated *in vivo* and the influence of heterogeneity of exosomes on distal barrier crossing.

Therefore, in the current study, we reported that (1) internalized ultrasmall NPs, namely ZnCdSe@ZnS quantum dots (QDs), could be secreted into the extracellular environment via Exo, a phenomenon observed both in macrophages J774A.1 and immortalized tumor HeLa cell, but with differences in efficiency, and (2) Exo encapsulation secreted from tumor cells enhanced the ability of QDs to cross the BBB.

https://doi.org/10.1021/acsnano.3c09378
ACS Nano XXXX, XXX, XXX−XXX

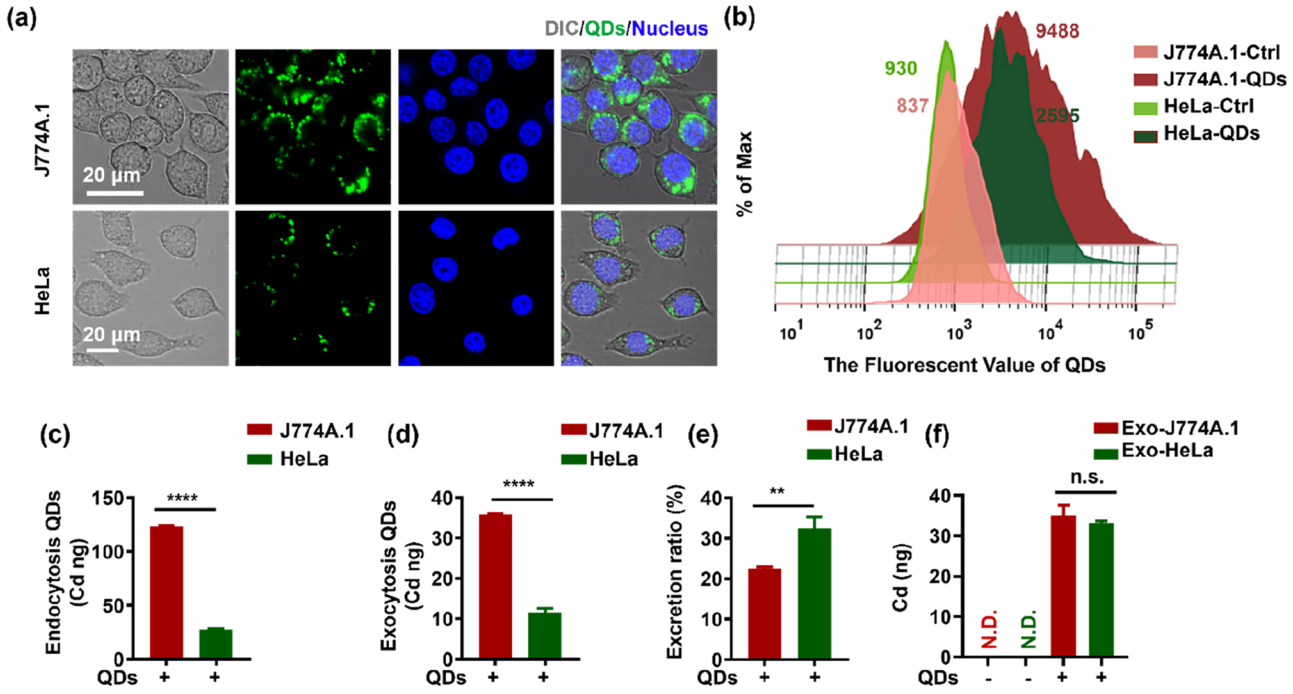

Figure 2. Quantification of QDs internalization and excretion. J774A.1 and HeLa cells (1×10^6) were incubated with 10 nM QDs for 12 h. (a) Intracellular QDs were imaged by CLSM. Scale bar, 20 μm. (b) The fluorescence intensity of intracellular QDs was quantified by FC. (c) The content of Cd was determined by ICP-OES. (d) After rinsing three times, cells were further cultured with FBS-free DMEM medium for an additional 24 h. Cells were then collected and digested for ICP-OES analysis. (e) Excretion ratio (%) of intracellular QDs = Exocytosis QDs/Endocytosis QDs × 100%. (f) J774A.1 and HeLa cells (1×10^7) were incubated with 10 nM QDs for 12 h. After removing excess QDs, cells were further cultured with FBS-free DMEM medium for an additional 48 h. Supernatants were collected to extract Exo by differential ultracentrifugation. After digestion, the content of Cd in Exo was detected by ICP-OES. All data are means ± SD ($n = 3$). An unpaired t-test was used. $^{**}p < 0.01$, $^{****}p < 0.0001$. No detection (N. D.) indicates that the amount of Cd was 0 μg/mL measured by ICP-OES. n.s., no significance.

Thus, this study implicated Exo encapsulation as a route for distal transport and "barrier-crossing" of NPs, further supporting the risk assessment of NPs under complicated scenarios. In addition, the advantage of active incorporation of NPs into biogenic origin Exo implied their potential biomedical applications.

RESULTS

Excretion of QDs via Extracellular Vesicle (EV) Encapsulation. ZnCdSe@ZnS QDs (average size of 8.4 ± 2.1 nm, the zeta potential of −31.5 ± 3.3 mV, Figure S1 in the Supporting Information) are used as a nanoparticle model because QDs are characterized and monodispersed with steady bright fluorescence. Furthermore, we have previous data on their interactions with cells, showing that they are readily internalized via cellular endocytosis and with a cell-independent pathway, then QDs subsequently distribute intracellularly and accumulate in lysosomes.[29] In addition, ZnS coating further enhanced the biocompatibility and stability,[30] which makes them excellent surrogates *in vivo* study.

As a cell model, we chose macrophages J774A.1 cells and tumor cells HeLa cell as the monocyte/macrophage's properties of J774A.1 cell and the bulky shape and easier transfection of HeLa. According to the cell counting kit-8 (CCK-8) assay, QDs showed decent biocompatibility in both macrophages (J774A.1) and tumor cells (HeLa). Significant cytotoxicity was not detected until the exposure concentration reached 100 nM (Figure S2). To avoid unwanted cytotoxicity that may affect further results, the exposure concentration of QDs was set at 10 nM (1/10 of the minimum effective cytotoxic dose) for the following *in vitro* experiments.

Once endocytosed, the intracellular NPs were wrapped and distributed in morphologically different endosomes and finally delivered into recycling endosomes for exocytosis[31] or into lysosomes to digest.[32] Here, early endosomes (labeled with early endosome antigen 1 antibody, EEA1), lysosomes (labeled with lysosomal associated membrane protein 2 antibody, LAMP 2), and autolysosomes (labeled with microtubule-associated protein 1 light chain 3 antibody, LC3) were individually blotted with Cy3 (red)-conjugated antibody to visualize the intracellular journey of QDs by confocal laser scanning microscopy (CLSM).[33,34] Obviously, orange-fluorescent dots were shown in the early endosome, lysosome, and autophagosome compartments, indicating their colocalization with QDs (green fluorescence). Apparent clusters of orange-fluorescent dots were abundant in the perinuclear region of lysosome in both J774A.1 and HeLa cells (Figure 1a and Figure S3). We further used super-resolution Nikon structured illumination microscopy (N-SIM) to confirm that QDs were colocalized with these organelles (Figure S4). Those results indicated that QDs had consistent intracellular fate in different cell types, thus transported intracellularly in the form of endosomal envelopment after endocytosis.

Since endosome-derived EVs are known to form first as intraluminal vesicles (ILVs) of internal multivesicular bodies (MVBs), and then move toward and undergo fusion with the plasma membrane to release cargoes into the extracellular space,[35−37] we stained the cell membrane with the red

https://doi.org/10.1021/acsnano.3c09378
ACS Nano XXXX, XXX, XXX−XXX

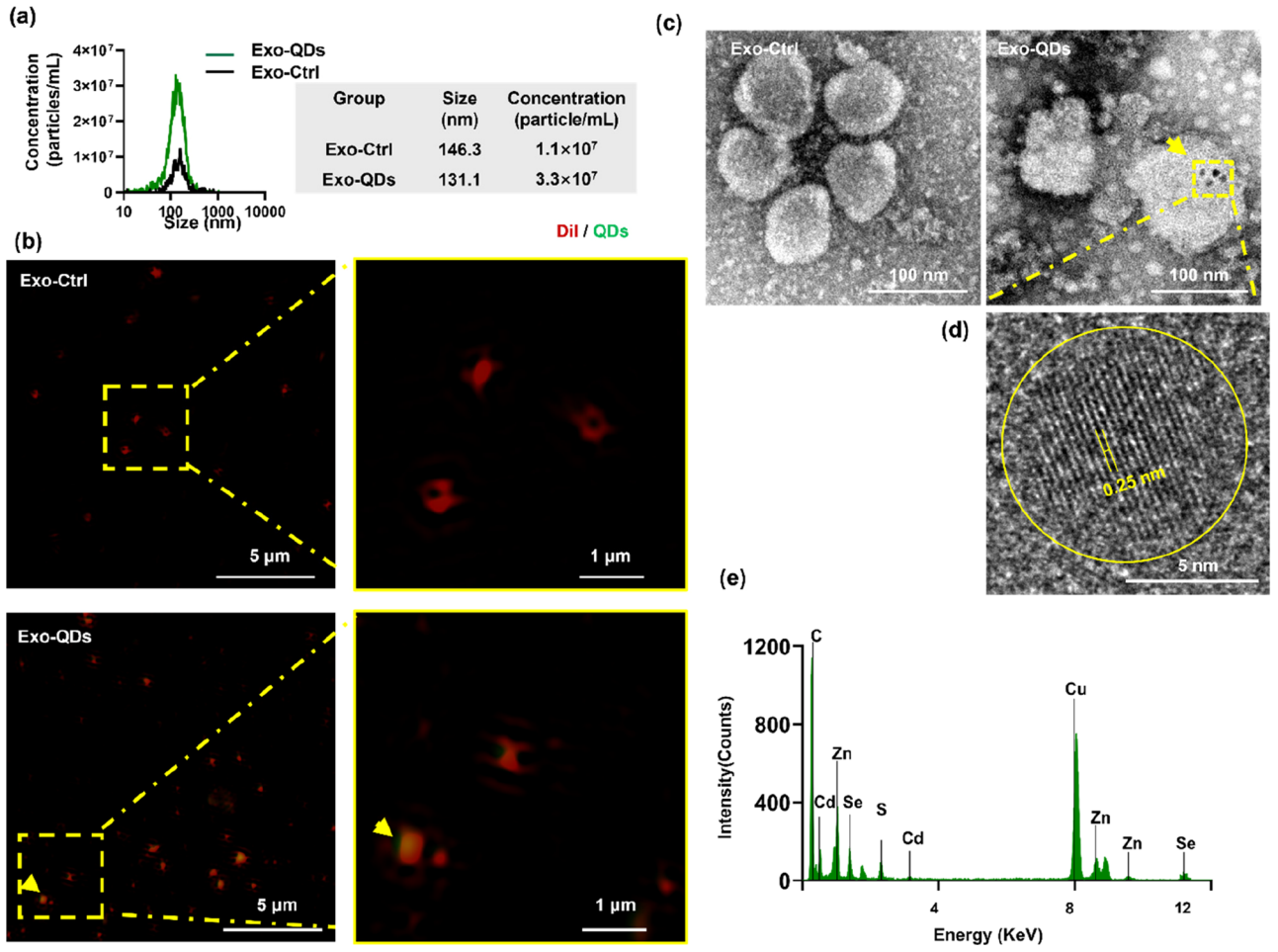

Figure 3. QDs were excreted along with Exo. J774A.1 cells (1×10^7) were incubated with 10 nM QDs for 12 h, and then free QDs were removed. The culture medium was replaced with an FBS-free medium for 48 h. Exo was obtained by differential ultracentrifugation from the cell supernatant. (a) Exo was diluted 1000 times in sterile PBS. The size and concentration of Exo were determined by NTA. (b) DiI (red) was used to stain Exo. Then, Exo was purified by a 100 kDa ultrafiltration tube (Millipore) and imaged by N-SIM. Scale bars, 5 and 1 μm. (c) TEM image of Exo, scale bar, 100 nm. (d) HRTEM images of QDs encapsulated in Exo. Scale bar, 5 nm. (e) In situ elements analysis of QDs encapsulated in Exo by EDS.

fluorescent dye 1,1′-dioctadecyl-3,3,3′,3′-tetramethylindocarbocyanine perchlorate (DiI) and found an elevated level of EVs (size of ~300 nm) adjacent to the cell membrane upon QDs stimulation (Figure 1b). To confirm the assumption that encapsulated QDs were secreted into extracellular space, cells were exposed to QD-containing medium, which was replaced with QDs-free medium afterward. The intracellular and extracellular fluorescent levels of QDs were measured and quantified (vs. untreated cells) to evaluate the amount of secretion. As indicated, the fluorescence intensity in the supernatant increased, while that in the cytoplasm decreased in a time-dependent manner (Figure 1c).

Exocytosis is a dynamic process of the intracellular vesicle system, which is the prominent and essential pathway for releasing intracellular cargo.[38,39] CD63, a transmembrane component of endosome, is abundant in MVBs, organelles involved in recycling routes between the plasma membrane and cellular vesicles.[37,40] We thus transfected a red fluorescent protein (RFP)-tagged CD63 into the HeLa cell line (CD63-RFP-HeLa) to monitor the real-time trajectories of internalized QDs.[41] Compared to scattered green QDs fluorescence in RFP-HeLa cells (negative control cell line), the concentrated orange-fluorescent spots in CD63-RFP-HeLa cells indicated the colocalization of CD63 protein with intracellular QDs (Figure S5). Interestingly, time-lapse confocal microscopy images (Figure 1d) and video (Video S1) demonstrated the concurrent inward (green to orange fluorescence, marked with white circles) and outward (orange to green fluorescence, marked with blue circles) movement of QDs, suggesting the dynamics involved in endocytosis and exocytosis of assembly QDs in CD63-enriched endosomes.

Exocytosis is an active transport process; thus, actin and microtubule cytoskeletons are necessary for the trafficking of intracellular cargo. To elucidate the role of exocytosis in the secretion of QDs, the cell-permeable actin polymerization inhibitor cytochalasin B (Cyto B) and microtubule inhibitor nocodazole were used to reduce cellular dynamism or traffic. GW4869, a common Exo biogenesis and release inhibitor, was used to block the budding of MVBs and release mature Exo from MVBs.[42,43] Inhibitor treatment increased the fluorescence intensity of cytoplasm and decreased the fluorescence intensity of supernatants in QD-exposed groups (Figure 1e and Figure S6), but without affecting cell survival rate (Figure S7). Here, we confirmed that intracellular QDs were encapsulated in CD63-enriched endocytic vesicles (early endosome, MVBs, lysosome, and autolysosome). Meanwhile, they were also, at

https://doi.org/10.1021/acsnano.3c09378
ACS Nano XXXX, XXX, XXX−XXX

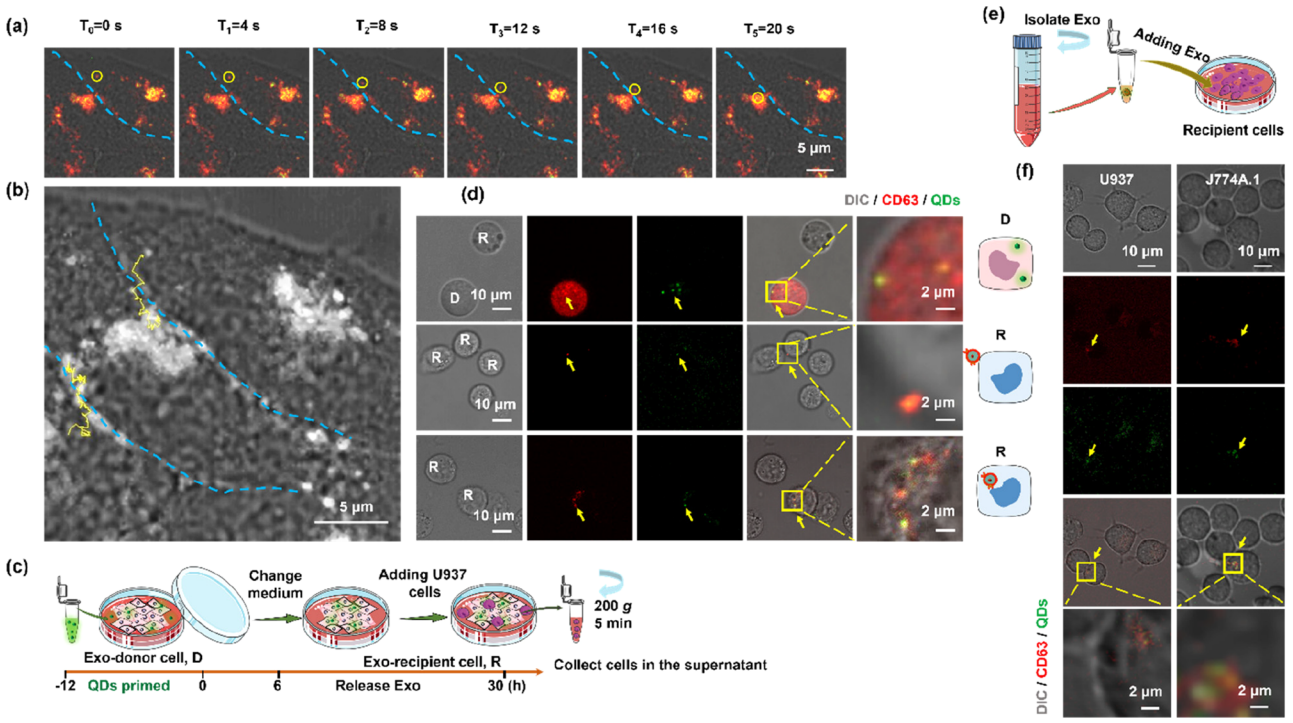

Figure 4. Intercellular communication of Exo-QDs. (a) Intracellular QDs were encapsulated in CD63-enriched endosomes and transferred between proximal CD63-RFP-HeLa cells. Cells were incubated with 10 nM QDs for 12 h. Time-lapse images were recorded with no-delay mode using CLSM. The intracellular trafficking route of QDs was encircled in yellow. Scale bar, 5 μm. (b) Trajectories of QDs' intercellular transfer between CD63-RFP-HeLa cells. Intracellular orange dots (CD63-enriched-endosome encapsulated QDs) were analyzed by Fiji plugin tracking. Scale bar, 5 μm. (c) Schematic illustration of a coculture system. In brief, CD63-RFP-HeLa cells (donor cells, D) were seeded into 10 cm dishes and incubated with 10 nM QDs for 12 h. After excess QDs were removed, the U937 cells (recipient cells, R) were then introduced to dishes and cocultured with CD63-RFP-HeLa cells at 37 °C for 24 h. Cells in the supernatant were collected for further analysis. (d) CD63-enriched-endosome encapsulated QDs (orange dots, as indicated by yellow arrowheads) in cells were imaged by CLSM. Scale bars, 10 and 2 μm. (e) Schematic illustration of intercellular communication of Exo-QDs. In brief, CD63-RFP-HeLa cells were incubated with 10 nM QDs for 12 h. After completely removing free QDs, FBS-free DMEM replaced the culture medium, and cells were cultured for a further 48 h. Supernatants were collected to isolate Exo. Purified Exo was added to the recipient cells and cocultured for another 2 h. (f) Exo-QDs (indicated by yellow arrowheads) in U937 or J774A.1 recipient cells were imaged by CLSM. Scale bars, 10 and 2 μm.

least in part, secreted into the extracellular environment along with Exo through exocytosis (Figure 1f).

Quantification of QD Internalization and Excretion. Next, we sought to quantify the percentage of internalized and excreted QDs in both J774A.1 and HeLa cells. For a direct comparison, J774A.1 and HeLa cells (1×10^6 cell/well) were incubated with 10 nM QDs for 12 h in parallel. As shown in Figure 2a, more green fluorescent dots were observed in J774A.1 cells compared to HeLa cells. By employing flow cytometry (FC) analysis, we found that the fluorescence value in QDs-treated J774A.1 cells (J774A.1-QDs) was ~3.6-fold more than that in the HeLa-QDs group (Figure 2b). For further quantification of internalized QDs, the content of cadmium (Cd) in cells was detected by inductively coupled plasma optical emission spectroscopy (ICP-OES). Approximately 37.6% (122.9 ng Cd) of total QDs (327.3 ng Cd, expressed in Cd) had been internalized in J774A.1 cells, while only 8.3% of QDs (27.56 ng Cd) were found in HeLa cells (Figure 2c). This result fully demonstrated that macrophages have a better ability to engulf QDs.

Exocytosis is the opposite function of endocytosis to maintain cellular homeostasis. The exocytosis of QDs was also detected in two types of cells. After 12 h of QDs treatment, cells were rinsed with PBS three times and cultured with FBS-free DMEM for 24 h. Cells were collected and digested, and the content of Cd was determined by ICP-OES. The difference in intracellular Cd% levels before and after FBS-free DMEM replacement indicated the amount of QDs released by exocytosis. The result showed that 10.9% (35.9 ng Cd) and 3.6% (11.6 ng Cd) of total QDs were secreted from J774A.1 and HeLa cells, respectively (Figure 2d). Interestingly, the excretion ratio of QDs (exocytosis/endocytosis) was higher in HeLa cells (42.2%) than that in J774A.1 cells (29.2%) (Figure 2e). A consistent study showed that cancerous cells secrete more EVs than noncancerous counterparts.[44] Various EVs, including Exo, microvesicles, microparticles, shedding vesicles, retrovirus-like particles, and apoptotic bodies, may involve exocytosis.[45,46] In addition, the excretion profile of NPs was mainly influenced by cell type.[47] A previous study demonstrated that Exo release from a noncancerous cell line was less than from a cancerous cell line.[48] This phenomenon was further confirmed in our study. Although the amounts of Exo from J774A.1 and HeLa cells without QD treatment are comparable, the concentration of Exo in the QD-treated HeLa cells was considerably increased over that of the QDs-treated J774A.1 cells (Figure S8). Intriguingly, we found that the amount of encapsulated QDs in Exo released by J774A.1 and HeLa were comparable (Figure 2f). Together, these results suggested the heterogeneity of

https://doi.org/10.1021/acsnano.3c09378
ACS Nano XXXX, XXX, XXX−XXX

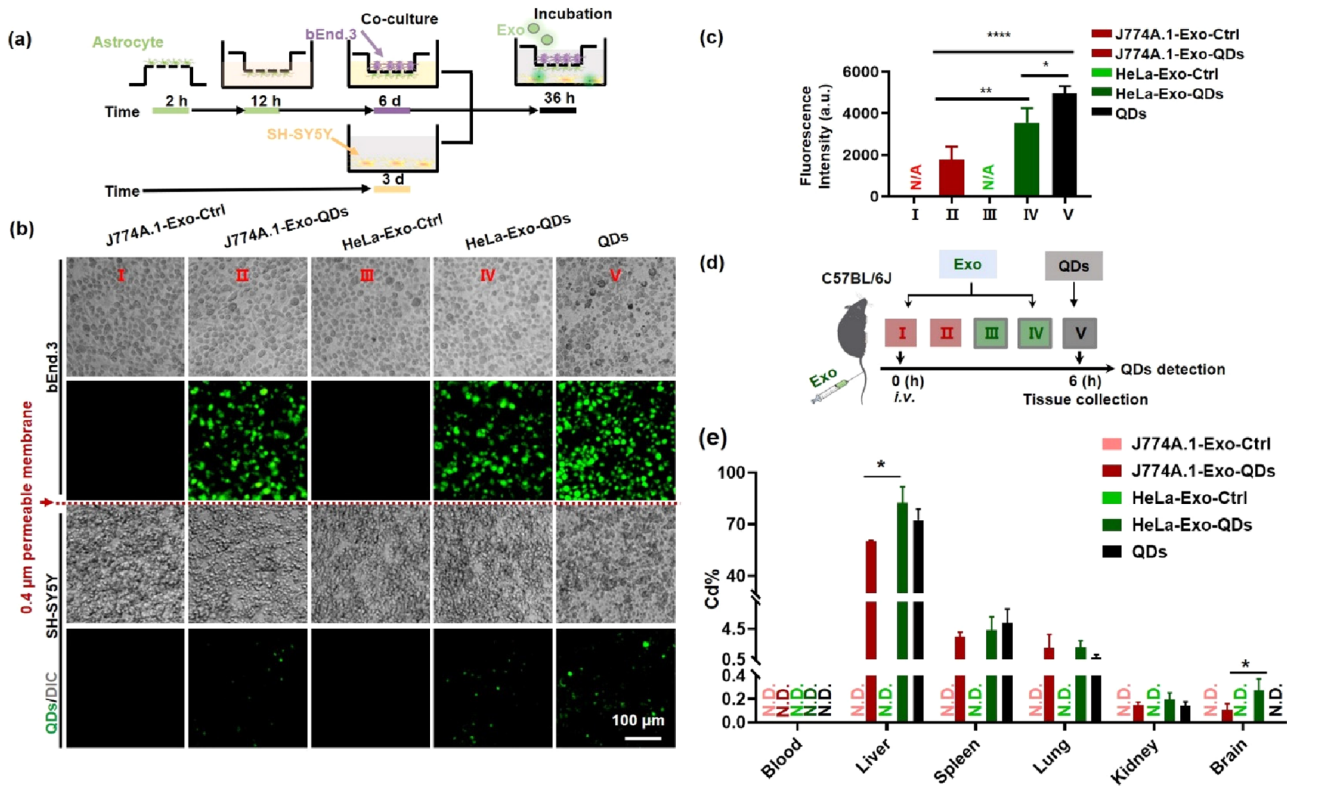

Figure 5. Exo encapsulation facilitates QD barrier-crossing trafficking. (a) Schematic representation of Exo-encapsulated QDs crossing BBB model *in vitro*. In brief, C8-D1A astrocytes (5×10^5 cells/cm^2) were seeded at the bottom of the microporous semipermeable membrane (transwell inserts). After adhering for 2 h, the insets were cultured in a 24-well plate for an additional 12 h. Then, bEnd.3 cells (1×10^6 cells/cm^2) were added to the upper side of the inset and cocultured with astrocytes for 6 days. Meanwhile, SH-SY5Y cells were seeded on the bottom of another 24-well culture plate for 3 days. Next, the insets were placed adjacent to a 24-well plate adhered with SH-SY5Y cells. Then, Exo or QDs were introduced to the insets and cocultured for 36 h. The bEnd.3 and SH-SY5Y cells were collected for further analysis. (b) Images of bEnd.3 and SH-SY5Y cells in the BBB model. Exo-QDs, or equivalent free QDs (0.3 μg of Cd), were incubated with bEnd.3 cells in the apical chamber. After coculturing, bEnd.3 and SH-SY5Y cells were collected and imaged by an inverted fluorescence microscope (×10, OLYMPUS, IX71). Scale bar, 100 μm. (c) The fluorescence intensity of intracellular QDs in SH-SY5Y cells was measured by Fiji software. An unpaired *t*-test was used. *$p < 0.05$, **$p < 0.01$, ****$p < 0.0001$. N/A indicates that no fluorescence intensity was detected. (d) Schematic diagram of Exo encapsulation facilitating QDs barrier-crossing trafficking *in vivo*. Exo collected from different groups, or an equal dose of QDs (4.5 μg of Cd), was respectively injected into C57BL/6J mice through the tail vein. After 6 h, mice were sacrificed, and tissues were collected for further analysis. (e) The content of Cd in different tissues was determined by ICP-OES. All data are means ± SD, $n = 3$. An unpaired *t*-test was used. *$p < 0.05$. No detection (N. D.) indicates that the amount of Cd was 0 μg/mL measured by ICP-OES.

QDs' internalization, cargo shorting, and excretion in different source cells.

QDs were Excreted Along with Exo. Since GW4869 inhibited the release of intracellular QDs to the extracellular environment (Figure 1e), we proposed that QDs were assembled into enclosed vesicles and secreted through Exo. To verify this hypothesis, corresponding Exo from J774A.1 macrophages were collected through differential ultracentrifugation[49] and subjected to nanoparticle tracking analysis (NTA). Biomarkers for Exo, including CD63, HSP70, HSP 90, and TSG101, were verified by Western blotting (Figure S9). The collected Exo have comparable particle sizes in the control and QDs groups (146.3 and 131.1 nm, respectively). Interestingly, the concentration of Exo tripled in the QDs group compared with the control group (Figure 3a). N-SIM (Figure 3b) and CLSM (Figure S10) analysis indicated orange-fluorescent foci in Exo that carry QDs (Exo-QDs) since only red fluorescence was observed in Exo from the control group (Exo-Ctrl). Consistently, transmission electron microscopy (TEM) analysis further confirmed the existence of QDs inside of the single-membrane vesicle (Figure 3c). In addition, high-resolution TEM (HRTEM) analysis clearly showed the crystalline structure of the Exo-QDs with a lattice spacing of 0.25 nm (Figure 3d). *In situ* energy dispersive X-ray (EDS) analysis validated the elementary composition of Zn, Cd, Se and S inside Exo-QDs (Figure 3e). Taken together, these results proved that QDs had been encapsulated in Exo and were then released into the extracellular environment. Exo can effectively deliver exogenous substances to distal target organs or cells. Recently, Exo has begun to be recognized as a safe and effective solution for drug delivery.[50] Substances, including therapeutic nucleic acids, proteins, lipids, and low molecular weight drugs, can be encapsulated into Exo passively or actively, where the active pathway involves the biogenesis of Exo. Here, we demonstrated that active strategies of cellular loading NPs into Exo; however, this active encapsulation has low efficiency.

Intercellular Communication of Exo-encapsulated QDs (Exo-QDs). Exo plays an essential role in cell−cell communication by allowing cells to exchange proteins, lipids, and genetic material.[51−53] A recent study report showed that Exo could mediate the transfer of atmospheric particulate matter actively between macrophages and induce inflammatory responses.[54] Another example demonstrated a delivery

https://doi.org/10.1021/acsnano.3c09378
ACS Nano XXXX, XXX, XXX−XXX

approach using NPs-loaded Exo generated by exocytosis from tumor cells.[55] Therefore, we speculated that cell-autonomous Exo-QDs from donor cells could be delivered to proximal or distal recipient cells. First, time-lapse confocal microscopy was utilized to investigate the movement of endocytic compartment-encapsulated QDs in CD63-RFP-HeLa cells. As indicated, during a period of 20 s, endocytic compartment-encapsulated QDs (orange fluorescent foci, marked with yellow circles) crossed a cell boundary (blue line) from an upper cell to a lower cell (Figure 4a and Video S2). We next employed single-particle tracking (SPT) to analyze the trajectory of individual encapsulated QDs, as shown in Figure 4b (marked with yellow lines) and Video S3. The results indicated that endocytic compartment-encapsulated QDs were delivered between adjacent cells.

Distal trafficking requires NPs to detach from primary tissue/cell into blood and extravasate. Thus, a coculture system was then established to further assess the transportation of released CD63-enriched-endosomes encapsulated QDs from donor cells to nonadjacent receptor cells within different cell types (Figure 4c). U937, a cell line exhibiting monocyte morphology and suspension was selected as the Exo receptor cells. Specifically, adherent CD63-RFP-HeLa cells (donor cell, D) were exposed to QDs for 12 h. Then, cells were thoroughly washed with PBS and cultured with fresh QDs-free medium for 6 h to eliminate excess QDs adsorbed on the cell membrane. After gently rinsing three times with PBS, suspension U937 cells (recipient cell, R) were added and cocultured with CD63-RFP-HeLa cells for an additional 24 h. As shown in Figure 4d, CD63-enriched-endosomes encapsulated QDs (orange-fluorescent dots) were observed both in donor and recipient cells.

Furthermore, to verify that Exo "carry" QDs for intercellular transport, rather than other EVs (micro vesicles, shedding vesicles, or apoptotic bodies) encapsulated QDs traffic, Exo were isolated from QDs-treated CD63-RFP-HeLa cells and then incubated with suspension U937 or adherent J774A.1 cells (Figure 4e). As expected, bright orange-fluorescent spots were seen in both living U937 and J774A.1 cells (Figure 4f). Three-dimensional reconstruction movie of Z-stacks in U937 (Video S4) and J774A.1 cells (Video S5) demonstrated intracellular orange-fluorescent dots, which strongly confirmed the presence of Exo-QDs in different recipient cells. On the contrary, only red fluorescent dots were observed in both types of cells when incubated with Exo obtained from untreated CD63-RFP-HeLa cells (Figure S11). Exo-QDs may enter recipient cells through various endocytic pathways, which are affected by proteins and receptors present on both Exo and recipient cells, such as exosomal integrins or scavenger receptor type B-1 on the cell surface.[56] The specific mechanism of endocytosed Exo is not discussed in this section.

Exo Encapsulation Facilitates QD Barrier-Crossing Trafficking. BBB is a uniquely functional, structural, and physiological interface between neuronal tissue and the peripheral blood supply. BBB plays an important role in maintaining central nervous system (CNS) homeostasis by restricting the transfer of toxic or harmful molecules and removing metabolites from the brain.[57] Since mounting evidence suggested Exo as a delivery vehicle for various materials across biological barriers,[58] we next explored the role of Exo encapsulation in QDs crossing the BBB. Endothelial bEnd.3 and astrocyte C8-D1A cells were cocultured in the transwell to mimic a BBB model (Figure 5a). Neuroblastoma SH-SY5Y cells were seeded on the bottom of the transwell as a recipient cell. Exo was introduced to the transwell insert and maintained for 36 h. Interestingly, a significant amount of green fluorescent dots was found in bEnd.3 cells, suggesting that Exo had been internalized by bEnd.3 cells via transcytosis or membrane fusion.[59] In the case of intact endothelial cells, the transcellular pathway plays a dominant role when tight junctions and adherens junctions block the paracellular pathway. Please note that Exo internalized into recipient cells by transcytosis was delivered to the endocytic membrane-compartments;[60] therefore, we asked if Exo were internalized into recipient cells via transcytosis. To address this question, Exo obtained from J774A.1 or HeLa cells with or without QDs treatment were stained with the lipophilic membrane dye DiI individually and purified before incubation with bEnd.3 cells. CLSM analysis indicated evenly distributed red fluorescence in Exo-Ctrl groups and a few orange-fluorescent dots in Exo-QDs groups (Figure S12). Furthermore, orange-fluorescent dots have also been observed in recipient SH-SY5Y cells (Figure S13). These results confirmed the transcytosis pathway in the endocytosed Exo between nonadjacent cells, followed by loading of Exo-QDs for presentation to recipient cells. Additionally, green fluorescent dots were observed in SH-SY5Y cells treated with Exo from QD-treated J774A.1 (J774A.1-Exo-QDs, group II) and HeLa cells (HeLa-Exo-QDs, group IV), but not Exo from control J774A.1 (J774A.1-Exo-Ctrl, group I) or HeLa (HeLa-Exo-Ctrl, group III) cells (Figure 5b). Notably, quantitative study indicated 2-fold green fluorescence in SH-SY5Y cells in group IV compared to group II (Figure 5c), suggesting the heterogeneity of Exo and tumor cell-derived Exo may own greater capacity of transcytosis. The fluorescence intensity of intracellular QDs in SH-SY5Y cells was also quantified by FC, the results were consisting with the quantitative analysis of fluorescence images (Figure S14). Of note, QDs alone (group V) could also be internalized into bEnd.3 and cross the bEnd.3/C8-D1A BBB model *in vitro* to reach the inner of recipient cells, and the largest QDs were detective probably related to the transcytosis of EVs, not only Exo.

Apparently, BBB endothelial cells are highly responsive to Exo from macrophages sources, which leads to higher BBB penetration of these Exo.[23] Furthermore, tumor-derived Exo can impair endothelial cell junctions and thus increase vascular permeability, establishing a favorable microenvironment for premetastatic niche formation and metastasis.[21,22] To provide more insight into how Exo heterogeneity affects QDs across the BBB, an *in vivo* animal model was adopted accordingly. As shown in Figure 5d, we directly injected Exo-QDs into C57BL/6J mice via the tail vein and quantified QDs (reflected by Cd%) in different tissues by ICP-OES. Exo dosages were normalized by their corresponding Cd content, and an equal dose of free QDs (4.5 μg of Cd) was used as a control. Most NPs are cleared from blood vessels and trapped in the mononuclear phagocyte system (MPS) after administration,[61] including QDs.[62] This phenomenon may explain the off-targeting of nanomedicine delivery strategies. In the current study, QDs were rapidly eliminated from systemic circulation. After 6 h of injection, no sign of Cd was detected in the blood via ICP-OES (Figure S15). As reported, QDs mainly accumulated in the mononuclear phagocytic system (MPS) organs in all groups (i.e., liver and spleen) (Figure 5e). As an endogenous vesicle, Exo ensures good biocompatibility in the systemic circulation.[63] In fact, the Cd% levels in HeLa-Exo-QDs and J774A.1-Exo-QDs are ~3- and ~2-fold more than

https://doi.org/10.1021/acsnano.3c09378
ACS Nano XXXX, XXX, XXX−XXX

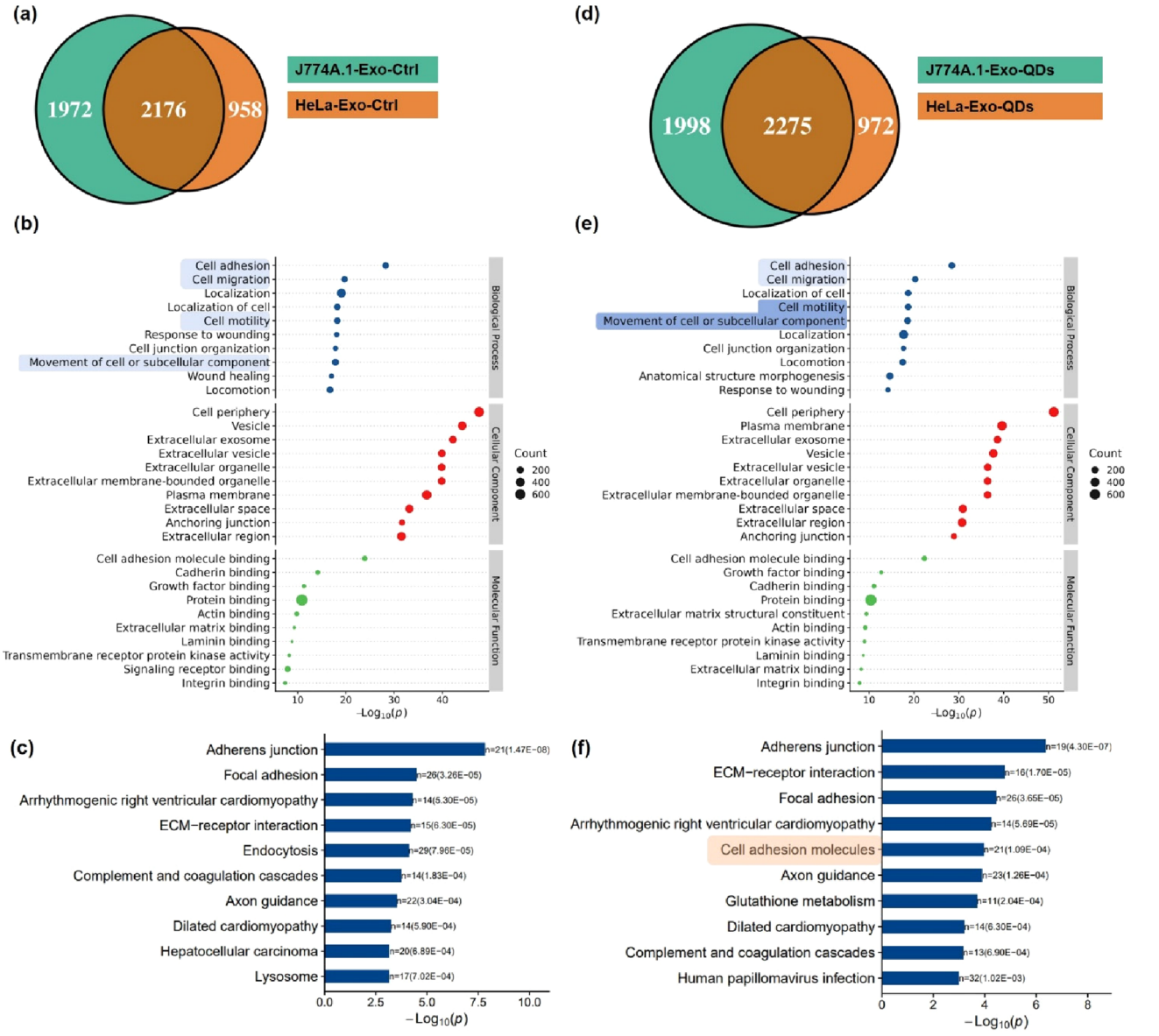

Figure 6. Protein composition and functional heterogeneity of Exo from different origins. (a, d) Venn diagrams of detected proteins in Exo derived from (a) J774A.1 and HeLa cells or (d) QD-treated J774A.1 and HeLa cells. (b, e) Unique proteins in Exo derived from (b) HeLa and (e) QD-treated HeLa cells underwent GO analysis. The horizontal coordinate is the negative logarithm of *p*-values shown for each GO term ($p < 0.05$), the vertical coordinate is the GO term, each circle represents a term, the size of the circle represents count, and different colors represent the BP, CC, and MF, respectively. (c, f) The top 10 enrichment pathways in Exo derived from (c) HeLa and (f) QD-treated HeLa cells underwent KEGG pathway analysis ($p < 0.05$); the horizontal coordinate is the negative logarithm of *p*-values, and the vertical coordinate is the enriched pathway. The number of proteins annotated in each pathway and *p*-value values are marked on the right side of the column.

those in the bare QDs group, respectively, at 2 min postinjection (Figure S15). Surprisingly, QDs could be detected in brain tissues with the Exo-QDs-administered groups (II and IV), rather than Exo-Ctrl groups (I and III) (Figure 5e). The content of Cd in the HeLa-Exo-QDs group (IV) accounted for approximately 0.3% of the total injected, but only 0.1% of the total injected in the J774A.1-Exo-QDs group (II). No sign of QDs was observed in the brain tissue of mice receiving direct injections of equal doses of free QDs (4.5 μg of Cd, V), which may be due to the rapid clearance of MPS.[64] In parallel, CLSM images of the frozen brain section also showed the green fluorescence of QDs in Exo-QDs groups (II and IV), but not in other groups. Quantitative fluorescence analysis showed that more QDs were detected in the HeLa-Exo-QDs group (Figure S16). Together, these results illustrated that QDs "hijack" Exo to achieve long-distance, barrier-crossing trafficking, and Exo from tumorous HeLa cells has better efficiency in crossing the BBB, further facilitating the translocation of QDs.

Protein Composition and Functional Heterogeneity of Exo from Different Origins. Exo is highly heterogeneous. Depending on the cell sources and biological environment, Exo can mediate both pathogenetic and therapeutic functions. Exo derived from metastasis were shown to contain cargo promoting migration, proliferation, invasion, and angiogenesis while nonmetastatic-Exo contained mostly proteins involved in cell−cell/cell-matrix adhesion and polarity maintenance.[65] Nevertheless, there is a surprising scarcity of data related to

https://doi.org/10.1021/acsnano.3c09378
ACS Nano XXXX, XXX, XXX−XXX

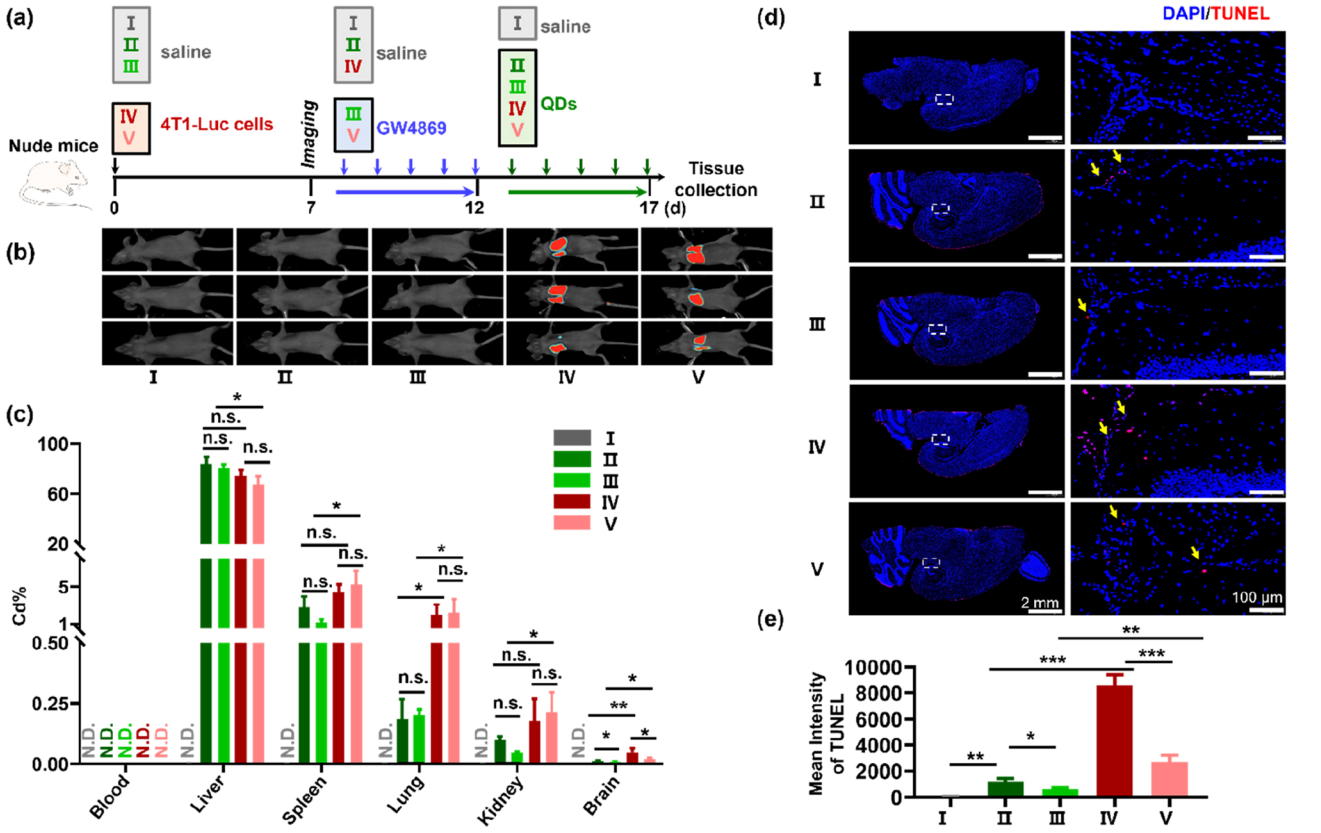

Figure 7. Tumor-derived Exo promotes the distal delivery of QDs. (a) Schematic diagram of animal treatment *in vivo*. In brief, female nude BALB/c mice were randomly divided into five groups. 1×10^6 4T1-Luc cells or 200 μL of normal saline were injected into mice via the tail vein. On the 7th day, D-luciferin (150 mg/kg) was intraperitoneally injected into mice, and then bioluminescence was imaged within 30 min by the NEWTON 7.0 Imaging System (Viber, France). On the 8th day, GW4869 (2.5 mg/kg/day) was intraperitoneally injected for 5 successive days. From the 13th day, QDs (5 mg/kg/d) were injected via the tail vein for 5 successive days. At 12 h postlast injection, mice were sacrificed, and tissues were collected. (b) The representative bioluminescent images of nude BALB/c mice were chosen. (c) Distribution of QDs in different tissues. The content of Cd was determined by ICP-OES. (d) Representative TUNEL staining images of brain slices with red fluorescent dots indicating the positive result. Scale bars, 2 mm and 100 μm. (e) Fluorescence quantification for TUNEL staining (n = 3). All data are means ± SD, n = 3. An unpaired t-test was used. *p < 0.05, **p < 0.01, ***p < 0.001. No detection (N.D.) indicates that the amount of Cd was 0 μg/mL measured by ICP-OES. n.s., no significance.

the compositional heterogeneity of Exo, and many fundamental questions remain.[66,67] We have shown that tumor cells-derived Exo is a higher efficiency delivery platform for translocating QDs from blood circulation to the brain tissue. Here, we explored the difference between protein composition and the biological function of Exo in macrophages and tumor cell sources to explain the compositional heterogeneity and ultimate utility in BBB crossing. Concretely, Exo from J774A.1 cells and HeLa cells with or without QDs treatment were isolated via differential ultracentrifugation, and the protein composition was quantified by the 4D label-free quantitative proteomics method. A total of 4148 and 3134 proteins were detected in Exo from J774A.1 cells (Table S1) and HeLa cells (Table S2), respectively. Venn diagram application tools are used for unions and intersections between different protein data sets from proteomics.[68] As shown in Figure 6a, there were 958 unique proteins present in Exo from HeLa cells, and 1972 unique proteins present in Exo from J774A.1 cells. Gene Ontology (GO) analysis was further performed to compare the functional protein composition of Exo. Through the GO annotations, specific gene products (proteins) are assigned to the specific ontology term of biological processes (BP), cellular components (CC), and molecular functions (MF). Exo from HeLa cells was enriched in the cellular functional proteins of cell adhesion, cell migration, and cell motility (Figure 6b), while Exo from J774A.1 cells was enriched in biological regulation, regulation of the cellular process and antigen processing (Figure S17). Furthermore, the top 10 terms enriched in the KEGG pathway analysis were differentially in Exo obtained from HeLa and J774A.1 cells. Specifically, adherens junction, ECM-receptor interaction, axon guidance and others were enriched in Exo from HeLa cells (Figure 6c), whereas complement and coagulation cascades, graft-versus-host disease, allograft rejection, and others were enriched in Exo from J774A.1 cells (Figure S18). Notably, adherens junction proteins play a critical role in regulating the permeability of the BBB,[69] ECM-receptor interaction is involved in the circulating Exo to mediate brain metastases,[70] axon guidance proteins are related to inflammatory response and endothelial function in CNS.[71] These results suggested that different sources of Exo are highly heterogeneous in terms of protein composition and function, and Exo derived from HeLa cell correlates more strongly with BBB homeostasis.

To examine how QDs influence protein enrichment in different sources of Exo, we also analyzed the protein composition and function in Exo derived from QDs-treated J774A.1 and HeLa cells. A total of 4273 and 3247 proteins were detected in Exo from QDs-treated-J774A.1 cells (Table

https://doi.org/10.1021/acsnano.3c09378
ACS Nano XXXX, XXX, XXX−XXX

S3) and QDs-treated-HeLa cells (Table S4), respectively. Among them, 28 up-expressed and 97 down-expressed proteins were found in HeLa Exo that received QDs (HeLa-Exo-Ctrl *v.s.* HeLa-Exo-QDs), while 178 up-expressed and 134 down-expressed proteins were found in J774A.1 Exo that received QDs (J774A.1-Exo-Ctrl *v.s.* J774A.1-Exo-QDs). Bioinformatics analysis, including GO and KEGG pathway analysis, were drawn to analyze the significantly differentially expressed proteins (DEPs, $p < 0.05$ and fold change >1.5 or <0.67) between the Exo from untreated cells and QDs-treated cells, the results showed that the biological processes of neither the DEPs derived from HeLa cell nor those derived from J774A.1 cells were enriched in cell adhesion, cell migration, and cell motility, as well as the pathways associated with physiological barriers crossing (Figure S19). In addition, the number of unique proteins slightly increased in the J774A.1-Exo-QDs and HeLa-Exo-QDs groups (Figure 6d). The top 10 GO enriched terms (Figure 6e) and the top 10 KEGG enriched terms (Figure 6f) remained constant to the Exo derived from HeLa cells without QDs treatment. Exo derived from QD-treated J774A.1 cells exhibited a similar phenomenon (Figure S20). Notably, the *p*-value values and number of proteins annotated in each enriched GO term and KEGG pathway differed. Specifically, KEGG analysis indicated further enrichment of cell adhesion molecule-related proteins in the unique proteins of the HeLa-Exo-QDs group.

To further analyze the DEPs that might contribute to the delivery of Exo (and their cargo) across the BBB, we performed an extended analysis of cell adhesion-associated DEPs in Exo derived from HeLa after QDs treatment (Table S5). As shown in Figure S21, CDH3, PLXNB2, CCL5, AMIGO2, and STXBP3 were up-expressed, while NRP2, PCK1 and PTEN were down-expressed. The result indicated that these DEPs might serve as potential biomarkers for crossing the biological barrier of Exo that originated from QDs-treated HeLa cells.

Together, a comprehensive protein characterization of Exo obtained from two cell lines (macrophages J774A.1 and tumor HeLa cell) confirmed Exo's heterogeneity. The unique protein contents from HeLa cell-derived Exo were implicated in regulating the barrier crossing-associated biological processes, such as cell adhesion, migration, and motility. Tumor cell-derived Exo has similar surface protein expressions compared with their parent cells; therefore, they still possess the nature of cancer cells, such as immunomodulation, proliferation, metastasis, and epithelial-mesenchymal transition.[53,72] Proteomic profiling of Exo from MDA-MB-231 cells exhibited protein binding, transferase activity.[73] Certain GO terms, such as binding and cell adhesion functions, were enriched in Exo original from U87 glioblastoma and Huh7 hepatocellular carcinoma cells.[74] In addition, EVs secreted from macrophages present molecular profiles associated with a Th1/M1 polarization signature, enhanced inflammation and immune response.[75]

Tumor-Derived Exo Promotes the Distal Delivery of QDs. Exo could migrate to distal parts and pass through the BBB[76] to propagate oncogenic signaling, including forming a premetastatic niche and manipulating distant microenvironments.[77] Here, we assumed that tumor-derived Exo was related to the accumulation of QDs in distal brain tissues. Most studies have focused on the *in vitro* transport of NPs; however, the internal environment can be rather complicated. To verify our above-mentioned discoveries *in vivo*, 4T1-Luc breast cancer xenograft mice model was set to assess the crossing barriers effect of tumor cell-derived Exo. Specifically, nude BALB/c mice were randomly divided into five groups and injected with saline (groups I, II, and III) or 4T1-Luc cells (a luciferase-expressing 4T1 cell line which was stably transfected with firefly luciferase gene, groups IV and V) via the tail vein (Figure 7a). On the seventh day, significant bioluminescence was observed in the lung of nude mice that had received 4T1-Luc cells, suggesting the successful setup of the 4T1-Luc breast cancer xenograft model (Figure 7b). From the eighth day, Exo inhibitor GW4869 was intraperitoneally injected into the mice of groups III and V for 5 successive days. From the 13th day, QDs were injected into groups II, III, IV, and V mice via the tail vein for 5 successive days. There has been no sign of tumor metastasis or invasion of the brain at the end of treatment. After harvest, the amount of QDs in different tissues, as reflected by Cd%, was quantified by ICP-OES. As expected, QDs were mainly accumulated in the liver and spleen in all groups, and trace amounts of QDs in the kidney and brain were also found. Surprisingly, lung tumor tissue (groups IV and V) accumulated more QDs than normal lung tissue (groups II and III). Furthermore, compared with group II, group IV showed significantly higher levels of QDs in the brain, suggesting the effect of tumor-derived Exo on the distal delivery of QDs *in vivo*. Meanwhile, various factors associated with breast cancer mice itself, such as the expression of vascular endothelial growth factor VEGF,[78] intercellular adhesion molecule 1 ICAM-1[79] and its associated molecule CD44[80] can promote trans-endothelial migration. The enhanced QDs delivery to the brain in the 4T1 model might also associated with the characteristics of the 4T1 model itself. GW4869, a common Exo biogenesis and release inhibitor, was used to block the budding of MVBs and release mature Exo.[42,43] It is reported that GW4869 treatment effectively inhibited Exo secretion in mice and could protect mice from developing experimental autoimmune myocarditis,[81] myeloma bone disease,[82] and ischemic injury.[83] In our study, pretreatment of GW4869 decreased the content of QDs in the brain (group III vs. group II, group V vs. group IV) (Figure 7c), further confirming that tumor-derived Exo could promote the distal delivery of QDs.

QDs containing Cd, a toxic heavy metal and a potential carcinogen, may have undesirable effects when QDs accumulate in organisms.[84] In addition, the physical properties of NPs, such as particle size, surface charge, and composition, may also contribute to negative biological responses. Multiple studies have shown that CdTe and CdSe@ZnS QDs could cross tissue barriers and accumulated in the tests, leading to oxidative stress, inflammation, cell apoptosis, and damage the tissue structures after administration QDs to mice by tail vein.[85,86] However, a low dose of CdTe and CdSe@ZnS QDs is relatively safe for the male reproductive system of mice.[85] The dosage of QDs (5 mg/kg/d BW) into the tail vein of mice in this study was based on the toxicity evaluation of CdSe@ZnS in the reference.[85,86] To correlate the internal exposure levels of QDs with their deleterious effects on the brain, brain sections were stained with a TUNEL staining kit. As shown in Figure 7d, QD-exposed groups (II, III, IV, and V) showed evident TUNEL-positive cells (red dots, as indicated by yellow arrowheads), indicating apoptotic cells, and elevated red dots are shown in the 4T1-Luc-treated groups (group IV vs. group II, group V vs. group III). Moreover, GW4869 pretreatment significantly reduced the number of TUNEL-positive cells

https://doi.org/10.1021/acsnano.3c09378
ACS Nano XXXX, XXX, XXX−XXX

(group III vs. group II, group V vs. group IV). Quantitative analysis of mean red fluorescence intensity also showed the same tendency (Figure 7e).

These results illustrated that Exo facilitates the translocation of QDs and that Exo from tumorous cells have better efficiency in crossing the BBB. The production of Exo is highly dependent on the environment, specifically by the induction of cell stress, such as hypoxia, heat, electric current, oxidative stress, pharmaceutics, or neoplastic conditions.[23] Here, we found that the QDs challenge simulates Exo production and programs cells to encapsulate QDs as payload. As removing unwanted intracellular contents is one of the most critical functions for Exo, the assembly of QDs in Exo can be considered not only an active manner to eliminate QDs but also a strategy of intercellular communication, especially tissue barrier trafficking, executed by QDs.

CONCLUSION

This study provides a proof-of-concept that Exo-mediated transport could serve as a mechanism for the distal effect of NPs. Our findings suggest that (1) Both macrophages J774A.1 and immortalized tumor HeLa cells can spontaneously load intracellular QDs into endosomes and releasing them as Exo-encapsulated-NPs by exocytosis. (2) Exo "carry" QDs for intercellular transport and even distal tissue barrier-crossing trafficking. (3) Tumor-derived Exo promotes the BBB crossing trafficking of QDs due to the protein composition and functional heterogeneity of Exo. Understanding how NPs actively break through the BBB is critical to both the biomedical applications and the risk assessment of NPs.

METHODS

Materials. Rabbit monoclonal LC3 (APG8B) antibody (Cat. No. SAB1306611, 1:200 dilution) was obtained from Sigma-Aldrich, and rabbit monoclonal EEA1 antibody (Cat. No. EPR4245, 1:200 dilution) was obtained from Abcam. Mouse monoclonal LAMP2 (H4B4) antibody (Cat. No. sc-18822, 1:200 dilution) and nocodazole (Cat. No. 31430−18−9) were purchased from Santa Cruz Biotechnology. GW4869 (Cat. No. 6823−69−4) was purchased from Selleck Chemicals. Cytochalasin B (Cyto B, Cat. No. 14930−96−2) was purchased from Aladdin Industrial Corporation. ZnCdSe@ZnS quantum dots (QDs, Cat. No. QS525) were obtained from Wuhan Jiayuan Quantum Dots Co., Ltd. Standard cadmium ion solution (1.0 mg/mL) (Cat. No. GZBZ1407−2016) was purchased from TMRM Standard Material Center. Hoechst 33342 (Cat. No. C1022) and DiI (Cat. No. C1036) for cell imaging was obtained from Beyotime Biotechnology. EndoFectin Max Transfection Reagent (Cat. No. EF013) was purchased from GeneCopoeia. Puromycin (Cat. No. 58−58−2) was obtained from Solarbio Sci & Tech Co., Ltd. Transwell plates (Cat. No. con-3413, 24-well, 6.5 mm diameter, 0.4 μm pore, polyester membrane inserts) were obtained from Corning Incorporated. TUNEL assay kits (G1502) were obtained from Servicebio Technology Co., Ltd.

Cell Culture. Murine macrophage cells J774A.1 (TIB-67) and HEK293T/17 (CRL-11268) used in this study were obtained from the ATCC (Shanghai, China). HeLa (TChu187), U937 (TChu159), and astrocyte (C8-D1A) cells were obtained from Army Medical University (Chongqing, China). bEnd.3 (BNCC337672) was obtained from BeNa Culture Collection (Henan, China). SH-SY5Y (CL-0208) was purchased from Procell Life Science &Technology Co., Ltd. (Wuhan, China). The 4T1-Luc cell line was constructed for a previous study.[87] J774A.1, HEK 293T/17, and HeLa cell lines were cultivated in Dulbecco's Modified Eagle's Medium (DMEM, Gibco). U937 cells were cultured in Roswell Park Memorial Institute 1640 (RPMI-1640, Gibco). The bEnd.3 and C8-D1A cells were cultured in DMEM/F12 (Gibco), and SH-SY5Y cells were cultured in MEM/F12 (Procell). All culture media were supplemented with 2 mM L-glutamine, 100 U/mL penicillin, 100 μg/mL streptomycin, 110 mg/L sodium pyruvate, and 10% fetal bovine serum (FBS, Gibco) and maintained in a humidified incubator containing 5% CO_2 at 37 °C.

TEM. QDs solution was dispersed on a copper grid with an ultrathin carbon film. The Exo solution was mounted on a thin film of amorphous carbon deposited on a copper grid and stained with uranyl acetate/lead citrate. After the solutions were dried at room temperature, the QDs and Exo size and morphology were examined on a Hitachi TEM (HT7800, Japan). HRTEM and *in situ* EDS of QDs encased in Exo were performed using a JEM-2100F microscope equipped with EDS spectrometry.

Hydrodynamic Size and Zeta Potential. Hydrodynamic size and zeta potential of QDs were measured with a Zetasizer instrument (Malvern Instruments, Nano ZS ZEN 3600, UK).

QD Exposure. Cells were seeded into 6-, 24-, and 48-well plates or 3.5 mm or 10 mm dishes at a suitable concentration and allowed to grow overnight. After incubating with 10 nM QDs, cells and supernatants were collected, respectively. Cells were prepared for cell counting kit-8 (CCK-8), Western blotting, immunofluorescence, flow cytometry, inductively coupled plasma optical emission spectrometry (ICP-OES) or imaging analysis, and supernatants were used for fluorescence intensity detection or Exo collection. For exocytosis inhibition assay, after cells were incubated with 10 nM QDs for 12 h, the culture medium was discarded to remove possible existing Exo, then replaced with FBS-free DMEM containing 5 μM GW4869, 33 μM nocodazole, or 10 μM Cyto B for 24 h.

CCK-8 Assay. CCK-8 (Bimake, USA, Cat. No. B34302) was used to determine cell viability. After incubating with QDs and inhibitors, cells were washed once with warm PBS. Then, the supernatant was replaced with an FBS-free DMEM medium containing 10% CCK-8 reagent. The plates were maintained at 37 °C for 2 h, and the corresponding absorbances at 450 nm were recorded on a SpectraMax iD3 microplate reader (Molecular Devices, San Jose, CA, USA).

Construction of CD63-RFP-HeLa Cells. Lentivirus was produced by transfecting a three-plasmid vector system comprised of a shuttle plasmid (pLVX-DsRed-Monomer-N1, blank) or (CD63-RFP, target plasmid) and two packaging plasmids (psPAX2 and pMD2.G) into HEK293T/17 cells as described previously.[88] Viral titer was determined by fluorescence analysis of infected HEK293T/17 cells. Lentiviral infection was conducted using 10 μL of virus per dish to infect 30−50% of HeLa cells. The overexpression of CD63-RFP in HeLa cells was observed with an inverted fluorescence microscope (Olympus, IX73).

Immunofluorescence Staining. Cells were incubated with 10 nM QDs for 2 h, and after being washed three times with PBS, cells were fixed with 4% paraformaldehyde at room temperature for 20 min. After rinsing three times with PBS, cells were permeabilized with 0.1% Triton X-100 in PBS for 10 min at room temperature. 10% bovine serum albumin (BSA) in PBS was used to block cells. Then, cells were incubated with the primary antibody overnight at 4 °C and the secondary antibody conjugated with Cy3 (red) for an additional 2 h at room temperature.

CLSM and N-SIM. Confocal images were recorded using the Nikon Eclipse Ti2 confocal imaging microscope (Nikon, Tokyo, Japan) equipped with a 60×, 1.40 NA, oil-immersion objective. Super-resolution images were recorded using a Nikon N-SIM super-resolution microscope (Nikon, Tokyo, Japan) equipped with a 100×, 1.49 NA, oil-immersion objective.

QD Tracking. To visualize the dynamic tracking of endocytic QDs, real-time dynamic analysis was performed on CLSM. Sequential image series at 16 bits were collected by selecting a region of interest of 128 × 128 pixels. Live cell time course analysis was performed in no-delay mode. Image stacks of at least 900 frames were collected, and the track of intracellular QDs was determined and analyzed on Fiji plugin tracking software. Three-dimensional reconstruction of Z-stacks was acquired with a Z-axis step of 0.18 μm. For SPT analysis, the linking range was set to 3 to bridge over short QDs blinking events (fewer than 3 frames), and the linking distance was chosen by

https://doi.org/10.1021/acsnano.3c09378
ACS Nano XXXX, XXX, XXX−XXX

15 pixels to ensure smooth linking. All individual trajectories greater than 10 frames were selected for further analysis.

Exo Extraction. J774A.1 cells were plated in 10 cm dishes (1×10^7 cells per dish) overnight and incubated with 10 nM QDs. After 12 h incubation, cells were washed with warm PBS three times to remove excess QDs and subsequently cultured in FBS-free DMEM medium for 6 h for further endocytosis of QDs. Then, the medium was discarded and replaced with a fresh FBS-free DMEM medium. After 48 h culture, cell supernatants were harvested to extract Exo. Differential ultracentrifugation is currently the gold standard method of Exo isolation.[89] Supernatants were differentially centrifuged at 500 *g*, 4 °C, 10 min twice, 2000 *g*, 4 °C, 30 min twice, and 10 000 *g*, 4 °C, 30 min. Then, supernatants were collected and passed through a 0.45 μm filter. Subsequently, the supernatants were ultracentrifuged at 110 000 g, 2 h twice (Optima L-100 XP Ultracentrifuge, Beckman Coulter) to pellet Exo. Finally, the collected Exo were resuspended in 100 μL of PBS and frozen at −80 °C for further analysis.

NTA. A Zeta view nanoparticle tracking analyzer (Particle Metrix, Germany) was used to measure the distribution and concentration of isolated Exo. Exo was diluted 1000 times in sterile PBS and injected into the analyzed chamber. Videos were acquired, and 11 positions were chosen using Zeta View 8.05.04 software. Isolated Exo underwent NTA before being stored at −80 °C until further analysis.

ICP-OES. Cells, Exo, and tissue samples were digested with a digestion solution (HNO_3:H_2O_2 = 3:1, v/v) at 65 °C for 12 h. Cd content was determined by ICP-OES (Avio 200, PerkinElmer, MA, USA).

Flow Cytometric Analysis. After QDs and inhibitor treatment, cells were analyzed by a BD Melody FACS (BD Biosciences, San Jose, CA, USA). Data were analyzed using FlowJo v10 software (FlowJo LLC data analysis software, Ashland, OR, USA).

***In Vitro* BBB Model.** Transwell chambers (6.5 mm with 0.4 μm pore polyester membrane inserts) were used to establish the *in vitro* BBB model. In brief, C8-D1A astrocyte cells (5×10^5 cells/cm^2) were seeded at the bottom of the microporous semipermeable membrane (transwell inserts). After adhering for 2 h, the insets were cultured in a 24-well plate for 12 h. Then, bEnd.3 cells (1×10^6 cells/cm^2) were added to the upper side of the inset and cocultured with astrocyte cells for 6 days. Meanwhile, SH-SY5Y cells were seeded onto the bottom of another 24-well culture plate for 3 days. The insert was placed adjacent to the 24-well plate, and then Exo or QDs were added to the insets and cocultured for 36 h. The bEnd.3 and SH-SY5Y cells were collected for further analysis.

Animal Care and Treatment. C57BL/6J and nude BALB/c mice were obtained from the Experimental Animal Center of Chongqing Medical University (Chongqing, China), bred, and held under specific pathogen-free (SPF) conditions. Mice were maintained on a 12/12 h light/dark cycle at a fixed temperature (23 °C) and humidity (50%) with free access to food and water. Animal experiments were approved by the Institutional Animal Care and Use Committee of Southwest University (IACUC-20211115−01), following the National Institutes of Health guidelines. Mice were allowed to acclimatize for 1 week before the experiment. For the Exo injection assay, Exo (from control or QDs-treated cells), or an equal dose of QDs (4.5 μg of Cd), was injected into C57BL/6J mice through the tail vein, mice were sacrificed after 6 h, and tissues were collected for further analysis. To verify the distal delivery of tumor-derived Exo, nude BALB/c mice were first injected with 1×10^6 4T1-Luc cells via the tail vein to create a breast tumor mouse model. On the seventh day, mice received intraperitoneal (*i.p.*) injection of D-luciferin (150 mg/kg), and corresponding bioluminescent images were acquired within 30 min using the NEWTON 7.0 Imaging System (Viber, France). On the eighth day, GW4869 (2.5 mg/kg/d) was *i.p.* injected into mice for 5 successive days. On the 13th day, QDs (5 mg/kg/d) were injected into mice via the tail vein for 5 consecutive days. Mouse tissues were collected for further investigation 12 h after the last injection.

TUNEL Staining. The brains of mice were cut into 5 μm thin sections after being embedded in paraffin. Then, sections were stained with the TUNEL Assay Kit to examine apoptotic cells according to the manufacturer's instructions (Servicebio, Wuhan, China). Briefly, sections were incubated with TUNEL reaction buffer (TDT enzyme: dUTP: buffer = 1:5:50) at 37 °C for 2 h in the dark, after which sections were deparaffinized and rehydrated, followed by antigen retrieval and permeabilization. DAPI was used to stain the nuclei. Sections were examined by fluorescence microscopy using a Nikon Eclipse Ci microscope equipped with a Nikon DS-U3 microscopy imaging system. Fluorescence quantification was performed by Fiji plugin tracking software.

Proteomics. Proteins were extracted from Exo samples (n = 3) and quantified with a bicinchoninic acid (BCA) protein assay kit. Protein (80 μg for each sample) digestion was performed with filter-aided sample preparation (FASP) method. The peptide was desalted with C18 Cartridge for further LC-MS analysis by Shanghai Bioprofile Technology Co., Ltd. Peptides were loaded on a trap column (75 μm × 250 mm, 1.6 μm, IonOpticks) in buffer A (0.1% formic acid in water) and eluted at a flow rate of 300 nL/min with a linear gradient from 98% solvent A (0.1% formic acid in water) to 80% solvent B (0.1% formic acid in 80% acetonitrile) for 60 min on an Easy-nLC1200 UHPLC system (Thermo Fisher Scientific). Data acquisitions were performed on a timsTOF ultra mass spectrometer (Bruker) using a positive ion mode with a scanning range of 100−1700 m/z. The intensity threshold was set at 5000.0, and Ion mobility was set at 0.6−1.6 Vs/cm^2 with a ramp time of 100.0 ms and accumulation time of 2.0 ms. Quadrupole isolation width was 2 m/z for m/z < 700 to 3 m/z for m/z > 700. Each TIMS cycle time was 1.1 s, including 1 Full MS and 10 PASEF MS/MS. Raw data files were processed with MSFragger before using Uniprot to search against the Uniprot_Mus musculus (Mouse) and Uniprot_Homo sapiens (Human) protein databases. Applied search parameters were fully tryptic with 2 missed cleavages, precursor tolerances of 20 ppm, and MS/MS tolerances of 20 ppm. Carbamidomethyl cysteine was set as a fixed modification, while acetylation of protein N-terminal, oxidation of methionine was set as variable modifications. The database search results were filtered and exported with a 0.01 false discovery rate (FDR) at peptide-spectrum-matched and protein levels, respectively. Razor and unique peptides were used for protein quantification. Only proteins with fold change ≥1.5-fold and a p-value <0.05 were considered for significantly differential expressions.

Bioinformatics Analysis. Microsoft Excel, Perseus software, and R statistical computing software were used to analyze the bioinformatics data. Hierarchical clustering analysis was performed with the "pheatmap package". The formation was extracted from the Kyoto Encyclopedia of Genes and Genomes (KEGG), and Gene Ontology (GO) was used to annotate the sequences. GO and KEGG enrichment analyses were carried out with Fisher's exact test, and FDR correction for multiple testing was also performed. Enriched GO and KEGG pathways were nominally statistically significant at p 0.05.

Statistical Analysis. The significance of the results was tested with a one-way analysis of variance (ANOVA) with Tukey multiple comparison test correction or unpaired t-test. Figures were assembled using GraphPad Prism, version 7 (GraphPad Software, Inc., La Jolla, CA, USA). Adjusted p values were calculated with SPSS 13.0, and differences were considered significant at $p < 0.05$. The data presented are representative of at least 3 independent repeats. Data with error bars are expressed as mean ± SD.

ASSOCIATED CONTENT

Data Availability Statement

The data that support the findings of this study are available from the corresponding authors upon reasonable request.

Supporting Information

The Supporting Information is available free of charge at https://pubs.acs.org/doi/10.1021/acsnano.3c09378.

Figure S1. Characterization of ZnCdSe@ZnS quantum dots (QDs). Figure S2. Cytotoxicity of QDs against J774A.1 and HeLa cells. Figure S3. Colocalization of QDs with intracellular vesicles. Figure S4. Colocalization of QDs with intracellular vesicles. Figure S5. Distribu-

https://doi.org/10.1021/acsnano.3c09378
ACS Nano XXXX, XXX, XXX−XXX

tion of QDs in CD63-RFP-HeLa cells. Figure S6. Inhibitors affected intracellular QDs secretion in HeLa cells. Figure S7. Cytotoxicity of inhibitors on cells. Figure S8. Quantitative analysis of Exo by NTA. Figure S9. Western blotting of Exo marker proteins. Figure S10. Visualization of Exo-encapsulated QDs. Figure S11. Exo driven from CD63-RFP-HeLa cells was captured by recipient cells. Figure S12. Exo were internalized into bEnd.3 cells via transcytosis. Figure S13. Exo were internalized into SH-SY5Y cells via transcytosis. Figure.S14. The fluorescence intensity of intracellular QDs in SH-SY5Y cells was quantified by FC. Figure S15. Blood circulation time of Exo-QDs and free QDs in mice. Figure S16. The presence of QDs in the frozen brain section of C57BL/6J mice. Figure S17. Unique proteins in Exo derived from J774a.1 cells underwent GO analysis. Figure S18. The top 10 enrichment pathways in Exo derived from J774a.1 cells underwent KEGG pathway analysis. Figure S19. GO analysis and KEGG pathway analysis of DEPs. Figure S20. Unique proteins in Exo derived from QDs-treated J774a.1 cells underwent GO analysis and KEGG pathway analysis. Figure S21. The heatmap for the differentially expressed proteins (DEPs) in Exo derived from QDs-treated HeLa cells associated with the cell adhesion biological process (PDF)

Video S1, transportation of QDs. (AVI)

Video S2, Transportation of Exo-QDs (AVI)

Video S3, single-particle trajectory (SPT) analysis of Exo-QDs (AVI)

Video S4, U937 cells subjected to three-dimensional reconstruction movie of Z-stacks (AVI)

Video S4, J774A.1 cells subjected to three-dimensional reconstruction movie of Z-stacks (AVI)

AUTHOR INFORMATION

Corresponding Author

Yang Song − *State Key Laboratory of Environmental Chemistry and Ecotoxicology, Research Center for Eco-Environmental Sciences, Chinese Academy of Sciences, Beijing 100085, China; Key Laboratory of Luminescence Analysis and Molecular Sensing, Ministry of Education, College of Pharmaceutical Sciences, Southwest University, Chongqing 400715, China;* orcid.org/0000-0001-7716-9216; Email: yangsong@rcees.ac.cn

Authors

Di Wu − *State Key Laboratory of Environmental Chemistry and Ecotoxicology, Research Center for Eco-Environmental Sciences, Chinese Academy of Sciences, Beijing 100085, China; Key Laboratory of Luminescence Analysis and Molecular Sensing, Ministry of Education, College of Pharmaceutical Sciences, Southwest University, Chongqing 400715, China; School of Pharmacy, Zunyi Medical University, Zunyi 563003, China*

Hang Sun − *State Key Laboratory of Environmental Chemistry and Ecotoxicology, Research Center for Eco-Environmental Sciences, Chinese Academy of Sciences, Beijing 100085, China; Key Laboratory of Luminescence Analysis and Molecular Sensing, Ministry of Education, College of Pharmaceutical Sciences, Southwest University, Chongqing 400715, China*

Bingwei Yang − *State Key Laboratory of Environmental Chemistry and Ecotoxicology, Research Center for Eco-Environmental Sciences, Chinese Academy of Sciences, Beijing 100085, China; Key Laboratory of Luminescence Analysis and Molecular Sensing, Ministry of Education, College of Pharmaceutical Sciences, Southwest University, Chongqing 400715, China*

Erqun Song − *Key Laboratory of Luminescence Analysis and Molecular Sensing, Ministry of Education, College of Pharmaceutical Sciences, Southwest University, Chongqing 400715, China;* orcid.org/0000-0003-4026-090X

Weihong Tan − *Molecular Science and Biomedicine Laboratory, State Key Laboratory for Chemo/Bio-Sensing and Chemometrics, College of Material Science and Engineering, College of Chemistry and Chemical Engineering, College of Biology, Hunan University, Changsha 410082, China; The Cancer Hospital of the University of Chinese Academy of Sciences (Zhejiang Cancer Hospital), Institute of Basic Medicine and Cancer (IBMC), Chinese Academy of Sciences, Hangzhou, Zhejiang 310022, China; Institute of Molecular Medicine, Renji Hospital, Shanghai Jiao Tong University School of Medicine, and College of Chemistry and Chemical Engineering, Shanghai Jiao Tong University, Shanghai 200240, China;* orcid.org/0000-0002-8066-1524

Complete contact information is available at: https://pubs.acs.org/10.1021/acsnano.3c09378

Notes

The authors declare no competing financial interest.

ACKNOWLEDGMENTS

This work is supported by the National Natural Science Foundation of China (22176206, 22174116), Chongqing Science Funds for Distinguished Young Scientists (cstc2021jcyj-jqx0024), and the Innovation Research Group at Higher Education Institutions in Chongqing, Chongqing Education Committee (CXQT21006). The authors thank Yuqi He (Zunyi Medical University) and Ming Xiao (Shanghai Bioprofile Technologe Company LTD, China) for advice on bioinformatics analysis.

REFERENCES

(1) Yang, W.; Wang, L.; Mettenbrink, E. M.; DeAngelis, P. L.; Wilhelm, S. Nanoparticle Toxicology. *Annu. Rev. Pharmacol Toxicol* **2021**, *61*, 269−289.

(2) Hochella, M. F.; Mogk, D. W.; Ranville, J.; Allen, I. C.; Luther, G. W.; Marr, L. C.; McGrail, B. P.; Murayama, M.; Qafoku, N. P.; Rosso, K. M. Natural, incidental, and engineered nanomaterials and their impacts on the Earth system. *Science* **2019**, *363* (6434), aau8299.

(3) Malysheva, A.; Lombi, E.; Voelcker, N. H. Bridging the divide between human and environmental nanotoxicology. *Nat. Nanotechnol* **2015**, *10* (10), 835−44.

(4) Liu, X. T.; Wei, W.; Liu, Z. X.; Song, E. Q.; Lou, J. L.; Feng, L. F.; Huang, R. C.; Chen, C. Y.; Ke, P. C.; Song, Y. Serum apolipoprotein A-I depletion is causative to silica nanoparticles-induced cardiovascular damage. *P Natl. Acad. Sci. USA* **2021**, *118* (44), e2108131118.

(5) Wei, W.; Li, Y. H.; Lee, M.; Andrikopoulos, N.; Lin, S. J.; Chen, C. Y.; Leong, D. T.; Ding, F.; Song, Y.; Ke, P. C. Anionic nanoplastic exposure induces endothelial leakiness. *Nat. Commun.* **2022**, *13* (1), 4757.

(6) Yan, Z.; Liu, Z.; Yang, B.; Zhu, X.; Song, E.; Song, Y. Long-term exposure of molybdenum disulfide nanosheets leads to hepatic lipid

accumulation and atherogenesis in apolipoprotein E deficient mice. *Nanoimpact* **2023**, *30*, 100462.
(7) Xu, D.; Ge, M.; Zong, M.; Wu, C.; Chen, Z.; Zhang, Z.; Zhu, Y.-X.; Lu, X.; Lin, H.; Shi, J. Revisiting the impacts of silica nanoparticles on endothelial cell junctions and tumor metastasis. *Chem.* **2023**, *9*, 1865.
(8) Pascual, F. Breaching the Barrier: Nanoscale Particulate Matter and Measures of Brain Health. *Environ. Health Perspect* **2021**, *129* (12), 124003.
(9) Qi, Y.; Wei, S.; Xin, T.; Huang, C.; Pu, Y.; Ma, J.; Zhang, C.; Liu, Y.; Lynch, I.; Liu, S. Passage of exogeneous fine particles from the lung into the brain in humans and animals. *Proc. Natl. Acad. Sci. U. S. A.* **2022**, *119* (26), No. e2117083119.
(10) Zhou, Y.; Peng, Z.; Seven, E. S.; Leblanc, R. M. Crossing the blood-brain barrier with nanoparticles. *J. Controlled Release* **2018**, *270*, 290−303.
(11) Herrmann, I. K.; Wood, M. J. A.; Fuhrmann, G. Extracellular vesicles as a next-generation drug delivery platform. *Nat. Nanotechnol* **2021**, *16* (7), 748−759.
(12) Sung, B. H.; von Lersner, A.; Guerrero, J.; Krystofiak, E. S.; Inman, D.; Pelletier, R.; Zijlstra, A.; Ponik, S. M.; Weaver, A. M. A live cell reporter of exosome secretion and uptake reveals pathfinding behavior of migrating cells. *Nat. Commun.* **2020**, *11* (1), 2092.
(13) Valadi, H.; Ekstrom, K.; Bossios, A.; Sjostrand, M.; Lee, J. J.; Lotvall, J. O. Exosome-mediated transfer of mRNAs and microRNAs is a novel mechanism of genetic exchange between cells. *Nat. Cell Biol.* **2007**, *9* (6), 654−9.
(14) Sun, X.; Xie, L.; Qiu, S.; Li, H.; Zhou, Y.; Zhang, H.; Zhang, Y.; Zhang, L.; Xie, T.; Chen, Y.; et al. Elucidation of CKAP4-remodeled cell mechanics in driving metastasis of bladder cancer through aptamer-based target discovery. *Proc. Natl. Acad. Sci. U. S. A.* **2022**, *119* (16), No. e2110500119.
(15) Berumen Sanchez, G.; Bunn, K. E.; Pua, H. H.; Rafat, M. Extracellular vesicles: mediators of intercellular communication in tissue injury and disease. *Cell Commun. Signal* **2021**, *19* (1), 104.
(16) Williams, C.; Palviainen, M.; Reichardt, N. C.; Siljander, P. R.; Falcon-Perez, J. M. Metabolomics Applied to the Study of Extracellular Vesicles. *Metabolites* **2019**, *9* (11), 276.
(17) Tian, X. Y.; Shen, H.; Li, Z. Y.; Wang, T. T.; Wang, S. J. Tumor-derived exosomes, myeloid-derived suppressor cells, and tumor microenvironment. *J. Hematol Oncol* **2019**, *12* (1), 84.
(18) Huang, C. Z.; Zhou, Y.; Feng, X. Y.; Wang, J. J.; Li, Y.; Yao, X. Q. Delivery of Engineered Primary Tumor-Derived Exosomes Effectively Suppressed the Colorectal Cancer Chemoresistance and Liver Metastasis. *ACS Nano* **2023**, *17* (11), 10313−10326.
(19) Alvarez-Erviti, L.; Seow, Y.; Yin, H.; Betts, C.; Lakhal, S.; Wood, M. J. Delivery of siRNA to the mouse brain by systemic injection of targeted exosomes. *Nat. Biotechnol.* **2011**, *29* (4), 341−5.
(20) Ferguson, S. W.; Nguyen, J. Exosomes as therapeutics: The implications of molecular composition and exosomal heterogeneity. *J. Controlled Release* **2016**, *228*, 179−190.
(21) Garcia-Roman, J.; Zentella-Dehesa, A. Vascular permeability changes involved in tumor metastasis. *Cancer Lett.* **2013**, *335* (2), 259−69.
(22) Hoshino, A.; Costa-Silva, B.; Shen, T. L.; Rodrigues, G.; Hashimoto, A.; Tesic Mark, M.; Molina, H.; Kohsaka, S.; Di Giannatale, A.; Ceder, S.; et al. Tumour exosome integrins determine organotropic metastasis. *Nature* **2015**, *527* (7578), 329−335.
(23) Rehman, F. U.; Liu, Y.; Zheng, M.; Shi, B. Exosomes based strategies for brain drug delivery. *Biomaterials* **2023**, *293*, 121949.
(24) Ohno, S.; Takanashi, M.; Sudo, K.; Ueda, S.; Ishikawa, A.; Matsuyama, N.; Fujita, K.; Mizutani, T.; Ohgi, T.; Ochiya, T.; Gotoh, N.; Kuroda, M. Systemically injected exosomes targeted to EGFR deliver antitumor microRNA to breast cancer cells. *Mol. Ther* **2013**, *21* (1), 185−91.
(25) Katakowski, M.; Buller, B.; Zheng, X.; Lu, Y.; Rogers, T.; Osobamiro, O.; Shu, W.; Jiang, F.; Chopp, M. Exosomes from marrow stromal cells expressing miR-146b inhibit glioma growth. *Cancer Lett.* **2013**, *335* (1), 201−4.
(26) Chen, L.; Charrier, A.; Zhou, Y.; Chen, R.; Yu, B.; Agarwal, K.; Tsukamoto, H.; Lee, L. J.; Paulaitis, M. E.; Brigstock, D. R. Epigenetic regulation of connective tissue growth factor by MicroRNA-214 delivery in exosomes from mouse or human hepatic stellate cells. *Hepatology* **2014**, *59* (3), 1118−29.
(27) Sancho-Albero, M.; Encabo-Berzosa, M. D. M.; Beltran-Visiedo, M.; Fernandez-Messina, L.; Sebastian, V.; Sanchez-Madrid, F.; Arruebo, M.; Santamaria, J.; Martin-Duque, P. Efficient encapsulation of theranostic nanoparticles in cell-derived exosomes: leveraging the exosomal biogenesis pathway to obtain hollow gold nanoparticle-hybrids. *Nanoscale* **2019**, *11* (40), 18825−18836.
(28) Sancho-Albero, M.; Navascues, N.; Mendoza, G.; Sebastian, V.; Arruebo, M.; Martin-Duque, P.; Santamaria, J. Exosome origin determines cell targeting and the transfer of therapeutic nanoparticles towards target cells. *J. Nanobiotechnology* **2019**, *17* (1), 16.
(29) Wu, D.; Zhu, X.; Ao, J.; Song, E.; Song, Y. Delivery of Ultrasmall nanoparticles to the cytosolic compartment of Pyroptotic J774A. 1 macrophages via GSDMDNterm membrane pores. *ACS Appl. Mater. Interfaces* **2021**, *13* (43), 50823−50835.
(30) McHugh, K. J.; Jing, L. H.; Behrens, A. M.; Jayawardena, S.; Tang, W.; Gao, M. Y.; Langer, R.; Jaklenec, A. Biocompatible Semiconductor Quantum Dots as Cancer Imaging Agents. *Advanced materials* **2018**, *30* (18), 1706356.
(31) Han, S.; da Costa Marques, R.; Simon, J.; Kaltbeitzel, A.; Koynov, K.; Landfester, K.; Mailander, V.; Lieberwirth, I. Endosomal sorting results in a selective separation of the protein corona from nanoparticles. *Nat. Commun.* **2023**, *14* (1), 295.
(32) Yang, Y.; Ning, H.; Xia, T.; Du, J.; Sun, W.; Fan, J.; Peng, X. Electrostatic Attractive Self-Delivery of siRNA and Light-Induced Self-Escape for Synergistic Gene Therapy. *Adv. Mater.* **2023**, *35* (30), No. e2301409.
(33) Flemming, J. P.; Hill, B. L.; Haque, M. W.; Raad, J.; Bonder, C. S.; Harshyne, L. A.; Rodeck, U.; Luginbuhl, A.; Wahl, J. K.; Tsai, K. Y.; et al. miRNA- and cytokine-associated extracellular vesicles mediate squamous cell carcinomas. *J. Extracell Vesicles* **2020**, *9* (1), 1790159.
(34) Issa, A.-R.; Sun, J.; Petitgas, C.; Mesquita, A.; Dulac, A.; Robin, M.; Mollereau, B.; Jenny, A.; Cherif-Zahar, B.; Birman, S. The lysosomal membrane protein LAMP2A promotes autophagic flux and prevents SNCA-induced Parkinson disease-like symptoms in the Drosophila brain. *Autophagy* **2018**, *14* (11), 1898−1910.
(35) Pegtel, D. M.; Gould, S. J. Exosomes. *Annu. Rev. Biochem.* **2019**, *88*, 487−514.
(36) Meldolesi, J. Exosomes and Ectosomes in Intercellular Communication. *Curr. Biol.* **2018**, *28* (8), R435−R444.
(37) Mathieu, M.; Nevo, N.; Jouve, M.; Valenzuela, J. I.; Maurin, M.; Verweij, F. J.; Palmulli, R.; Lankar, D.; Dingli, F.; Loew, D.; et al. Specificities of exosome versus small ectosome secretion revealed by live intracellular tracking of CD63 and CD9. *Nat. Commun.* **2021**, *12* (1), 4389.
(38) Hessvik, N. P.; Llorente, A. Current knowledge on exosome biogenesis and release. *Cellular & Molecular Life Sciences* **2018**, *75* (3), 193−208.
(39) Sahay, G.; Querbes, W.; Alabi, C.; Eltoukhy, A.; Sarkar, S.; Zurenko, C.; Karagiannis, E.; Love, K.; Chen, D.; Zoncu, R.; Buganim, Y.; Schroeder, A.; Langer, R.; Anderson, D. G. Efficiency of siRNA delivery by lipid nanoparticles is limited by endocytic recycling. *Nat. Biotechnol.* **2013**, *31* (7), 653−8.
(40) Pols, M. S.; Klumperman, J. Trafficking and function of the tetraspanin CD63. *Exp. Cell Res.* **2009**, *315* (9), 1584−92.
(41) Joshi, B. S.; de Beer, M. A.; Giepmans, B. N. G.; Zuhorn, I. S. Endocytosis of Extracellular Vesicles and Release of Their Cargo from Endosomes. *ACS Nano* **2020**, *14* (4), 4444−4455.
(42) Trajkovic, K.; Hsu, C.; Chiantia, S.; Rajendran, L.; Wenzel, D.; Wieland, F.; Schwille, P.; Brugger, B.; Simons, M. Ceramide triggers budding of exosome vesicles into multivesicular endosomes. *Science* **2008**, *319* (5867), 1244−7.

https://doi.org/10.1021/acsnano.3c09378
ACS Nano XXXX, XXX, XXX−XXX

(43) Verderio, C.; Gabrielli, M.; Giussani, P. Role of sphingolipids in the biogenesis and biological activity of extracellular vesicles. *J. Lipid Res.* **2018**, *59* (8), 1325−1340.
(44) Xu, R.; Rai, A.; Chen, M.; Suwakulsiri, W.; Greening, D. W.; Simpson, R. J. Extracellular vesicles in cancer - implications for future improvements in cancer care. *Nat. Rev. Clin Oncol* **2018**, *15* (10), 617−638.
(45) Akers, J. C.; Gonda, D.; Kim, R.; Carter, B. S.; Chen, C. C. Biogenesis of extracellular vesicles (EV): exosomes, microvesicles, retrovirus-like vesicles, and apoptotic bodies. *J. Neurooncol* **2013**, *113* (1), 1−11.
(46) Kubo, H. Extracellular Vesicles in Lung Disease. *Chest* **2018**, *153* (1), 210−216.
(47) Sakhtianchi, R.; Minchin, R. F.; Lee, K. B.; Alkilany, A. M.; Serpooshan, V.; Mahmoudi, M. Exocytosis of nanoparticles from cells: role in cellular retention and toxicity. *Adv. Colloid Interface Sci.* **2013**, *201−202*, 18−29.
(48) Riches, A.; Campbell, E.; Borger, E.; Powis, S. Regulation of exosome release from mammary epithelial and breast cancer cells - a new regulatory pathway. *Eur. J. Cancer* **2014**, *50* (5), 1025−34.
(49) Haraszti, R. A.; Didiot, M. C.; Sapp, E.; Leszyk, J.; Shaffer, S. A.; Rockwell, H. E.; Gao, F.; Narain, N. R.; DiFiglia, M.; Kiebish, M. A.; et al. High-resolution proteomic and lipidomic analysis of exosomes and microvesicles from different cell sources. *J. Extracell Vesicles* **2016**, *5*, 32570.
(50) Liang, Y.; Duan, L.; Lu, J.; Xia, J. Engineering exosomes for targeted drug delivery. *Theranostics* **2021**, *11* (7), 3183−3195.
(51) van Niel, G.; D'Angelo, G.; Raposo, G. Shedding light on the cell biology of extracellular vesicles. *Nat. Rev. Mol. Cell Biol.* **2018**, *19* (4), 213−228.
(52) Mathieu, M.; Martin-Jaular, L.; Lavieu, G.; Thery, C. Specificities of secretion and uptake of exosomes and other extracellular vesicles for cell-to-cell communication. *Nat. Cell Biol.* **2019**, *21* (1), 9−17.
(53) Kalluri, R.; LeBleu, V. S. The biology, function, and biomedical applications of exosomes. *Science* **2020**, *367* (6478), aau6977.
(54) Cui, X.; Lai, W.; Zhao, Y.; Chen, C. The Exosome-Mediated Cascade Reactions for the Transfer and Inflammatory Responses of Fine Atmospheric Particulate Matter in Macrophages. *Environ. Sci. Technol.* **2023**, *57* (21), 7891−7901.
(55) Yong, T.; Zhang, X.; Bie, N.; Zhang, H.; Zhang, X.; Li, F.; Hakeem, A.; Hu, J.; Gan, L.; Santos, H. A.; Yang, X. Tumor exosome-based nanoparticles are efficient drug carriers for chemotherapy. *Nat. Commun.* **2019**, *10* (1), 3838.
(56) Rufino-Ramos, D.; Albuquerque, P. R.; Carmona, V.; Perfeito, R.; Nobre, R. J.; Pereira de Almeida, L. Extracellular vesicles: Novel promising delivery systems for therapy of brain diseases. *J. Controlled Release* **2017**, *262*, 247−258.
(57) Bagchi, S.; Chhibber, T.; Lahooti, B.; Verma, A.; Borse, V.; Jayant, R. D. In-vitro blood-brain barrier models for drug screening and permeation studies: an overview. *Drug Des Devel Ther* **2019**, *13*, 3591−3605.
(58) Das, C. K.; Jena, B. C.; Banerjee, I.; Das, S.; Parekh, A.; Bhutia, S. K.; Mandal, M. Exosome as a Novel Shuttle for Delivery of Therapeutics across Biological Barriers. *Mol. Pharmaceutics* **2019**, *16* (1), 24−40.
(59) Heidarzadeh, M.; Gursoy-Ozdemir, Y.; Kaya, M.; Eslami Abriz, A.; Zarebkohan, A.; Rahbarghazi, R.; Sokullu, E. Exosomal delivery of therapeutic modulators through the blood-brain barrier; promise and pitfalls. *Cell Biosci* **2021**, *11* (1), 142.
(60) Tian, T.; Zhu, Y. L.; Hu, F. H.; Wang, Y. Y.; Huang, N. P.; Xiao, Z. D. Dynamics of exosome internalization and trafficking. *J. Cell Physiol* **2013**, *228* (7), 1487−95.
(61) Ngo, W.; Ahmed, S.; Blackadar, C.; Bussin, B.; Ji, Q.; Mladjenovic, S. M.; Sepahi, Z.; Chan, W. C. W. Why nanoparticles prefer liver macrophage cell uptake. *Adv. Drug Deliver Rev.* **2022**, *185*, 114238.
(62) Wang, H. J.; Yang, G. G.; Wu, S. S.; Meng, Z. F.; Zhang, J. M.; Cao, Y.; Zhang, Y. P. Toxicity of CuS/CdS semiconductor nanocomposites to liver cells and mice liver. *Sci. Total Environ.* **2021**, *784*, 147221.
(63) Tenchov, R.; Sasso, J. M.; Wang, X. M.; Liaw, W. S.; Chen, C. A.; Zhou, Q. A. Exosomes-Nature's Lipid Nanoparticles, a Rising Star in Drug Delivery and Diagnostics. *ACS Nano* **2022**, *16* (11), 17802−17846.
(64) Fam, S. Y.; Chee, C. F.; Yong, C. Y.; Ho, K. L.; Mariatulqabtiah, A. R.; Tan, W. S. Stealth Coating of Nanoparticles in Drug-Delivery Systems. *Nanomaterials (Basel)* **2020**, *10* (4), 787.
(65) Gangoda, L.; Liem, M.; Ang, C. S.; Keerthikumar, S.; Adda, C. G.; Parker, B. S.; Mathivanan, S. Proteomic Profiling of Exosomes Secreted by Breast Cancer Cells with Varying Metastatic Potential. *Proteomics* **2017**, *17* (23−24), DOI: 10.1002/pmic.201600370.
(66) Floriano, J. F.; Willis, G.; Catapano, F.; de Lima, P. R.; Reis, F. V. D. S.; Barbosa, A. M. P.; Rudge, M. V. C.; Emanueli, C. Exosomes Could Offer Options to Combat the Long-Term Complications Inflicted by Gestational Diabetes Mellitus. *Cells* **2020**, *9* (3), 675.
(67) Spitzberg, J. D.; Ferguson, S.; Yang, K. S.; Peterson, H. M.; Carlson, J. C. T.; Weissleder, R. Multiplexed analysis of EV reveals specific biomarker composition with diagnostic impact. *Nat. Commun.* **2023**, *14* (1), 1239.
(68) Jia, A.; Xu, L.; Wang, Y. Venn diagrams in bioinformatics. *Brief Bioinform* **2021**, *22* (5), bbab108.
(69) Bennett, C.; Samikkannu, M.; Mohammed, F.; Dietrich, W. D.; Rajguru, S. M.; Prasad, A. Blood brain barrier (BBB)-disruption in intracortical silicon microelectrode implants. *Biomaterials* **2018**, *164*, 1−10.
(70) Li, S.; Qu, Y.; Liu, L.; Zhang, X.; He, Y.; Wang, C.; Guo, Y.; Yuan, L.; Ma, Z.; Bai, H.; Wang, J. WITHDRAWN: Proteomic analysis of plasma-derived exosomes identifies biomarkers that distinguish brain and liver metastasis in lung cancer patients. *Cancer Lett.* **2022**, 215782.
(71) Zhou, Y. F.; Li, Y. N.; Jin, H. J.; Wu, J. H.; He, Q. W.; Wang, X. X.; Lei, H.; Hu, B. Sema4D/PlexinB1 inhibition ameliorates blood-brain barrier damage and improves outcome after stroke in rats. *Faseb J.* **2018**, *32* (4), 2181−2196.
(72) Lin, Z.; Wu, Y.; Xu, Y.; Li, G.; Li, Z.; Liu, T. Mesenchymal stem cell-derived exosomes in cancer therapy resistance: recent advances and therapeutic potential. *Mol. Cancer* **2022**, *21* (1), 179.
(73) Patwardhan, S.; Mahadik, P.; Shetty, O.; Sen, S. ECM stiffness-tuned exosomes drive breast cancer motility through thrombospondin-1. *Biomaterials* **2021**, *279*, 121185.
(74) Haraszti, R. A.; Didiot, M. C.; Sapp, E.; Leszyk, J.; Shaffer, S. A.; Rockwell, H. E.; Gao, F.; Narain, N. R.; DiFiglia, M.; Kiebish, M. A. High-resolution proteomic and lipidomic analysis of exosomes and microvesicles from different cell sources. *J. Extracell Vesicles* **2016**, *5*, 32570.
(75) Cianciaruso, C.; Beltraminelli, T.; Duval, F.; Nassiri, S.; Hamelin, R.; Mozes, A.; Gallart-Ayala, H.; Ceada Torres, G.; Torchia, B.; Ries, C. H.; et al. Molecular Profiling and Functional Analysis of Macrophage-Derived Tumor Extracellular Vesicles. *Cell Rep* **2019**, *27* (10), 3062.
(76) Jiang, Y.; Wang, F.; Wang, K.; Zhong, Y.; Wei, X.; Wang, Q.; Zhang, H. Engineered Exosomes: A Promising Drug Delivery Strategy for Brain Diseases. *Curr. Med. Chem.* **2022**, *29* (17), 3111−3124.
(77) Huang, Y.; Kanada, M.; Ye, J.; Deng, Y.; He, Q.; Lei, Z.; Chen, Y.; Li, Y.; Qin, P.; Zhang, J.; Wei, J. Exosome-mediated remodeling of the tumor microenvironment: From local to distant intercellular communication. *Cancer Lett.* **2022**, *543*, 215796.
(78) Lin, J.; Li, R.; Huang, Y.; Dilger, J. P.; Beto Mukherjee, M. Increased lung metastasis with sevoflurane in breast cancer surgery is associated with VEGF and elevated vascular permeability by VEGF in a mouse model of human breast cancer. *J. Clin Oncol* **2022**, *40* (16), e13060.
(79) Taftaf, R.; Liu, X.; Singh, S.; Jia, Y.; Dashzeveg, N. K.; Hoffmann, A. D.; El-Shennawy, L.; Ramos, E. K.; Adorno-Cruz, V.; Schuster, E. J.; et al. ICAM1 initiates CTC cluster formation and trans-endothelial migration in lung metastasis of breast cancer. *Nat. Commun.* **2021**, *12* (1), 4867.

https://doi.org/10.1021/acsnano.3c09378
ACS Nano XXXX, XXX, XXX−XXX

(80) Wang, P. C.; Weng, C. C.; Hou, Y. S.; Jian, S. F.; Fang, K. T.; Hou, M. F.; Cheng, K. H. Activation of VCAM-1 and its associated molecule CD44 leads to increased malignant potential of breast cancer cells. *Int. J. Mol. Sci.* **2014**, *15* (3), 3560−79.
(81) Sun, P.; Wang, N. X.; Zhao, P.; Wang, C.; Li, H. R.; Chen, Q.; Mang, G.; Wang, W. W.; Fang, S. H.; Du, G. Q.; Zhang, M. M.; Tian, J. W. Circulating Exosomes Control CD4 T Cell Immunometabolic Functions via the Transfer of miR-142 as a Novel Mediator in Myocarditis. *Mol. Ther* **2020**, *28* (12), 2605−2620.
(82) Faict, S.; Muller, J.; De Veirman, K.; Maes, K.; De Bruyne, E.; Schots, R.; Caers, J.; Vanderkerken, K.; Menu, E. Exosomes Play a Key Role in Multiple Myeloma Bone Disease and Tumor Development. *Blood* **2018**, *132*, 4484.
(83) Cheng, Z.; Garikipati, V. N. S.; Cimini, M.; Wang, C.; Trungcao, M.; Tang, Y.; Ye, Y.; Benedict, C.; Goukassian, D.; Verma, S. K; Kishore, R. Exosome Inhibition Improved Blood Perfusion in Ischemic Hindlimb of db/db Diabetic Mice. *Circ. Res.* **2017**, *121*, DOI: 10.1161/res.121.suppl_1.23.
(84) Li, L.; Tian, J. L.; Wang, X. M.; Xu, G. X.; Jiang, W. X.; Yang, Z. W.; Liu, D. M.; Lin, G. M. Cardiotoxicity of Intravenously Administered CdSe/ZnS Quantum Dots in BALB/c Mice. *Front. Pharmacol.* **2019**, *10*, DOI: 10.3389/fphar.2019.01179.
(85) Li, X. H.; Yang, X. R.; Yuwen, L. H.; Yang, W. J.; Weng, L. X.; Teng, Z. G.; Wang, L. H. Evaluation of toxic effects of CdTe quantum dots on the reproductive system in adult male mice. *Biomaterials* **2016**, *96*, 24−32.
(86) Li, L.; Lin, X. T.; Chen, T. T.; Liu, K.; Chen, Y. J.; Yang, Z. W.; Liu, D. M.; Xu, G. X.; Wang, X. M.; Lin, G. M. Systematic evaluation of CdSe/ZnS quantum dots toxicity on the reproduction and offspring health in male BALB/c mice. *Ecotox Environ. Safe* **2021**, *211*, 111946.
(87) Wang, Y.; Wang, Y.; Liu, Z.; Dong, W.; Yang, B.; Xia, X.; Song, E.; Song, Y. Polychlorinated Biphenyl Quinones Promotes Breast Cancer Metastasis through Reactive Oxygen Species-Mediated Nuclear Factor kappaB-Matrix Metalloproteinase Signaling. *Chem Res Toxicol* **2018**, *31* (9), 954−963.
(88) Lois, C.; Hong, E. J.; Pease, S.; Brown, E. J.; Baltimore, D. Germline Transmission and Tissue-Specific Expression of Transgenes Delivered by Lentiviral Vectors. *Science* **2002**, *295* (5556), 868.
(89) Haraszti, R. A.; Didiot, M. C.; Sapp, E.; Leszyk, J.; Shaffer, S. A.; Rockwell, H. E.; Gao, F.; Narain, N. R.; DiFiglia, M.; Kiebish, M. A.; Aronin, N.; Khvorova, A. High-resolution proteomic and lipidomic analysis of exosomes and microvesicles from different cell sources. *J Extracell Vesicles* **2016**, *5* (5), 32570.

https://doi.org/10.1021/acsnano.3c09378
ACS Nano XXXX, XXX, XXX−XXX